Journal of Materials Chemistry C

Exploiting the fraternal twin nature of thermoelectrics and topological insulators in Zintl phases as a tool for engineering new efficient thermoelectric generators

Journal:	*Journal of Materials Chemistry C*
Manuscript ID	TC-REV-02-2023-000556.R2
Article Type:	Review Article
Date Submitted by the Author:	01-May-2023
Complete List of Authors:	Ogunbunmi, Michael; University of Delaware, Chemistry and Biochemistry Bobev, Svilen; University of Delaware, Chemistry and Biochemistry

Journal of Materials Chemistry

ARTICLE

Exploiting the fraternal twin nature of thermoelectrics and topological insulators in Zintl phases as a tool for engineering new efficient thermoelectric generators

Received 00th January 20xx,
Accepted 00th January 20xx

DOI: 10.1039/x0xx00000x

www.rsc.org/

Michael O. Ogunbunmi[a], and Svilen Bobev*[a]

This review article presents a radical overview of the rich chemistry and physics of Zintl phases as it relates to their interesting structure-property relationships. In particular, it unveils the evolution of topological insulator (TI) and thermoelectric (TE) properties in Zintl materials as having a common origin and as such are driven by same materials properties ranging from narrow band gap to strong spin-orbit coupling effect. To this end, excellent TE properties are ubiquitous in many TIs and because of the ever-increasing interest in the studies of topological properties of matter, several robust theoretical frameworks now exist to provide us with additional intuitive nature and understanding of this exotic phase of matter. This invariably has also led to the screening of tens of thousands of materials for the presence of nontrivial topology using the combined predictive power of machine learning and ab-initio first-principles calculations. On the other hand, studies on TE materials are still largely based on some sort of hit-and-miss approach. Here we leveraged on the similar materials features and intersection between TE and TIs and review several Zintl materials that are already identified as TIs and presents how exploiting their bulk and surface states properties can be harnessed for developing highly efficient TE materials for practical purposes.

Introduction

Climate change and a drive towards the decarbonization of energy

The devastating effect of global warming and its attendant climate change, which among others include heat-waves, severe drought, and deadly floods, raging fires continues to stare at us in the face. Combating and mitigating these climate disasters appear to be a daunting task and yet our survival and that of the environment strongly depends on it. At the current rate of emission of greenhouse gases into the atmosphere, available data indicates a temperature rise of about 2.5°C towards the close of this century which is a milestone away from the target of 1.5°C.[1,2] A viable solution would no doubt require as much scientific intervention as international climate action plans and policies.

Despite all the efforts put in place over the years by the United Nations to get countries to commit to cutting down greenhouse gas emissions, it appears we would still experience a significant ~10.6 % increase in emission by 2030 as compared to that of year 2010.[1] By the UN Environment Program (UNEP), the only plausible pathway to achieving the target of keeping emission to 1.5°C is by cutting down greenhouse gas emission by up to 45 %.[3] Realizing this milestone will not be an easy feat to come by but it is certainly within reach provided there are concerted efforts towards environmental decarbonization and development of viable and efficient alternative/renewable sources of energy.[4]

One of the promising classes of materials envisioned to alleviate some of the above mentioned challenges are the thermoelectric materials. They can provide a clean source of energy via the recovery of waste heat and converting it into electricity. Thermoelectric materials can also be deployed for solid state refrigeration (or heat pumping) technologies as well, through the use of the Seebeck and Peltier effects, respectively.[5–7] For waste heat recovery applications, thermoelectric generators necessitate the use of materials that are stable and efficient at high-temperature; materials that are showing moderate/room temperature efficiencies are mostly suited for developing thermoelectric coolers.

Thermoelectric materials thus occupy a critical role in meeting up with the ever-increasing global energy demand and a pathway towards a decarbonized industrialization and development.[8] For example, it is estimated that between 17-20 % of the global energy consumption is from domestic and commercial cooling mostly from conventional vapor compression and up to 13 % of the global greenhouse gas emission by year 2030 would be from these refrigerating systems.[9,10] To this end, the drive towards solid state cooling devices based on Peltier effect and magnetocaloric effect

[a] Department of Chemistry and Biochemistry, University of Delaware, Newark, Delaware 19716, United States

which can offer a more environmentally friendly, reliability, cooling efficiency, compatibility, scalability, and low cost in comparison to the conventional vapor compression technology based on the Carnot cycle is on the rise.[11,12]

The thermoelectric effect and materials properties

The thermoelectric (TE) effect involves the direct conversion of temperature difference across two junctions into an electric voltage and vice versa, which is captured by the Seebeck and Peltier effects.[7,13] In line with the earlier discovery of Alessandro Volta,[14] in 1821, Thomas Johann Seebeck "rediscovered" the phenomenon in which he found that a voltage difference is produced across the junction of two dissimilar conductors (e.g. Cu and Bi).[15] When one of the two conducting materials is heated, the electrons become excited and move towards the cooler side of the other material, such that a direct current flows through when both materials are connected in the form of an electric circuit. Here the voltage generated is a function of the temperature difference across the two materials and can be of the magnitude of several millivolts for a large enough temperature difference. A typical TE device is made up of connecting several arrays of such materials electrically in series and thermally in parallel. The Peltier effect phenomenon on the other hand was discovered in 1834 by Jean Charles Peltier,[16] who found that there is a cooling (heat is absorbed) or heating (heat is liberated) at one junction of two dissimilar materials when the other junction is connected to an electric source, as such the Peltier effect can be considered as the reverse counterpart of the Seebeck effect. Similar to the Seebeck device, a Peltier heat pump would consist of such materials, arranged together in series—when current is passed through one of the junctions, hot and cold ends will be generated. Some other related thermoelectric effects are the Ettingshausen, Thomson and spin Seebeck effects,[17,18] but would not be covered in this article. The schematic representation of thermoelectric device based on Seebeck and Peltier effects are shown in Figure 1.

The TE performance of a material at a given operating temperature is characterized by the dimensionless figure of merit zT defined as:

$$zT = S^2\sigma T/\kappa \quad (1)$$

where S, σ, κ, and T are the Seebeck coefficient, electrical conductivity, thermal conductivity, and absolute temperature, respectively.[19] However, a stringent requirement applies for practical applications of TE materials, and in order to optimally harness their potential, a $zT \geq 1$ is required. To achieve this, candidate materials combining the features of high S and σ as well as low κ are desired. However, these three properties are mutually exclusive and are related to the charge carrier concentration n in a discordant nature that can simplify into an expression as: $n \propto \sigma/S\kappa$. A high S is achieved with low n, but this, in turn, leads to low σ such that improving one will compromise the other. A low n favors a high κ and a high S, whereas a high n favors a high σ.[19,20] A low κ and a high σ provides for the reduction of energy loss from conduction of heat and joule heating, respectively.

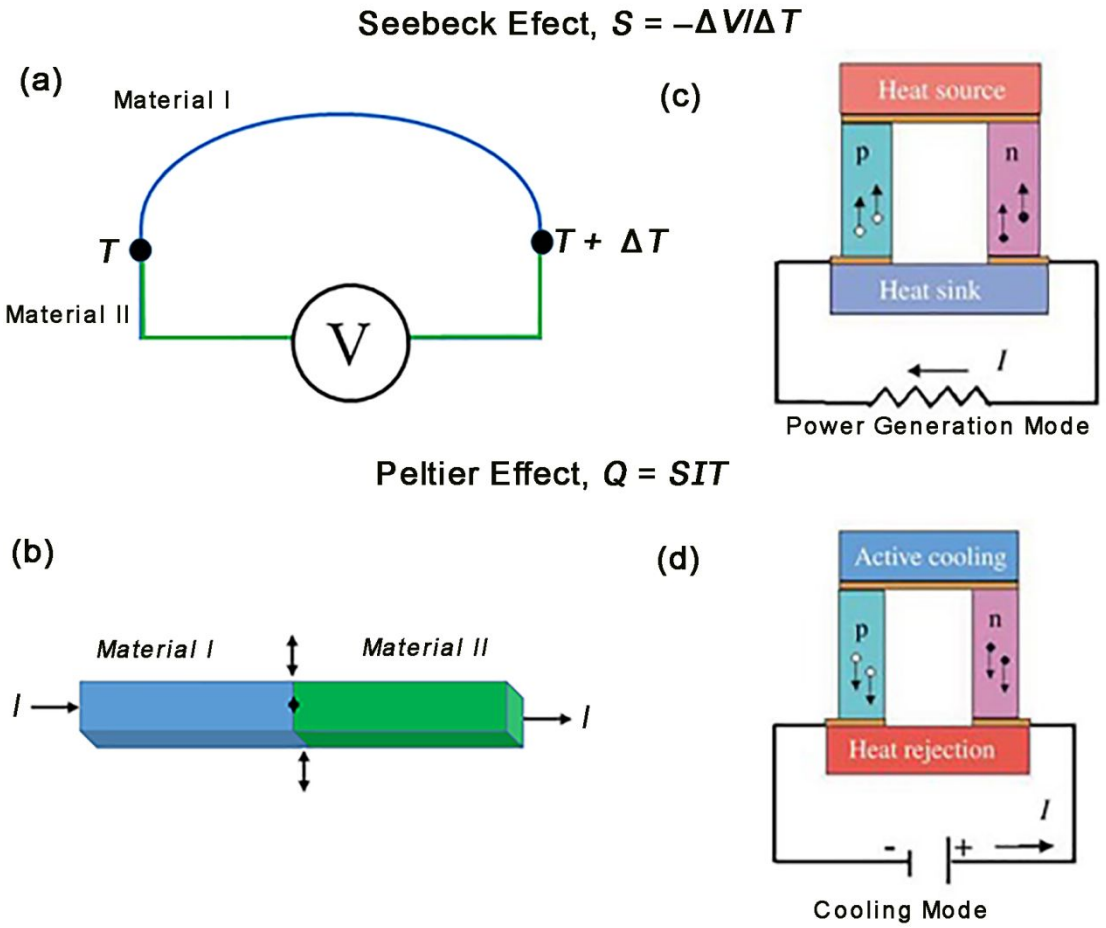

Figure 1. (a) The Seebeck effect and (b) Peltier effect illustrating the thermoelectric phenomena. (c) and (d) are the schematic representation of thermoelectric module for power generation and cooling modes, respectively. Figure adapted with permission from reference 21.

One of the innovative ways to surmount these conflicts is to identify suitable narrow band gap E_g semiconductors with heavy elements in addition to an inherent degree of disorder or complex atomic bonding. With a narrow E_g, a high carrier mobility can be achieved which leads to a relatively high σ. At the same time, a low κ may be achieved through an effective phonon scattering by high atomic mass elements, complex atomic bonding, and disorder in the material. In isotropic metals, the improvement on κ can be limited when the electronic thermal conductivity dominates over the lattice thermal conductivity based on the Wiedemann-Franz law.[22] However, such limitations are largely taken care off in semiconductors where κ is mostly dominated by the lattice contribution. Such a material can therefore be doped to tune n towards optimizing zT and as such most of the identified high-performance TE materials are degenerate semiconductors. It is noted that zT is optimized for n that lies at the border of those of semiconductors and metals. Therefore, narrow E_g materials where n falls between ca. 10^{19} and 10^{21} cm^{-3} are promising TE materials.[19] Other important considerations for a good TE material includes its ability to operate optimally or possess a high zT value over a wide temperature range which sets the efficiency limit of the material. Also, considerations such as toxicity, material stability, abundance and costs of constituent elements are important. Furthermore, the numerator of Eqn. 1 is the thermoelectric power factor $PF = S^2\sigma$, which can be used to access the maximum achievable power of a particular candidate material, is also often used to assess the TE performance.[23]

In recent years, there have been significant advancements in the development of TE materials. Various techniques such as the introduction of structural disorder, nanostructuring, grain size and grain boundary size tuning, phonon engineering, etc. have been used to achieve an ultra-low lattice thermal conductivity.[24,25] Also, the probe of the atomic dynamics such as the phonons interactions of these materials using local probe techniques such as neutron scattering can also provide an intuition into the phonon-phonon interaction and how to control phonon transport in a beneficial way. Other approaches involve improving the power factor through band engineering which can be used to achieve high density of state (DOS) and valley degeneracy.[23] Perhaps a more crucial aspect of the various techniques used in achieving low thermal conductivity and which is also an important consideration for topological insulators, has to do with using heavy elements to

drive phonon scattering. Further discussions on this aspect will be presented in the subsequent sections (*vide infra*).

The Zintl phases

Zintl phases are an important class of materials in solid-state sciences and refer to compounds that lie at the border of the typical valence precise salts and the intermetallics. The coinage of the name has its root in the earlier works of Eduard Zintl from the 1930s on compounds comprising of alkali and alkaline-earth metals (the least electronegative elements, denoted as *A* and *AE* hereafter) and the electronegative main group elements of group 13 and 14.[26] In those classic cases such as NaTl and NaPb, the electropositive sodium atoms donate their valence electrons to the electronegative Tl and Pb to achieve a closed-shell noble gas electronic configuration. Tl and Pb accept those electrons, which are insufficient to reach electron-octets; in turn the post-transition elements achieve stable electronic configurations by forming covalent bonds. The same principles hold true for other examples of typical Zintl phases, where the structures can be broken down to cations and (poly)anions, in which the electronic configuration of the cations and anions follow valence rules.[27,28] Over the years, the number of structurally characterized Zintl phases has grown,[29–35] although most examples of such compounds have remained as laboratory curiosity. However, over the course of the last 15-20 years, Zintl phases have received significant recognition from the thermoelectric community in particular, following the demonstration of unprecedented TE performance in Zintl antimonides.[36–38] This interest led to the rapid expansion of Zintl phases into the realm of transition and rare-earth elements; when such elements of open core-shells are incorporated, the attendant structural diversity and physical properties can reach new heights.[20,30,39–44]

The actualization of closed-shell electronic configuration in these materials brings about their characteristic features as semiconductors or insulators as well as the diamagnetic or temperature independent diamagnetic behavior.[26] The Zintl phases combine the features of narrow band gap, intricate atomic bonding and amenability to high degree of disorder and present a fertile playground to explore the various electronic and transport properties of materials of interests ranging from the topological phases of matter[45,46] to applications in thermoelectrics[47] and photovoltaics.[48,49] Leveraging on the idea of the Zintl-Klemm concept[50] thus allows for a myriad of opportunities to both conceptualize, design, and grow new materials at the heart of cutting-edge technological applications. More intuitively, the Zintl-Klemm concept allows for exploring the various structure-property relationships and the subsequent optimization of such properties from the understanding of the electron counts and bonding. To this end, there have been numerous investigations of these phases as they present suitable electronic and transport environments that can favor the realization of enhanced TE performance.[36] It suffices to note that one of the current state-of the-art TE material currently been used by NASA for space exploration is $Yb_{14}MnSb_{11}$[51] can be considered as a Zintl phase. Some other notable Zintl phases with excellent TE properties include $Ca_9Zn_{4+x}Sb_9$,[52] $YbCd_{2-x}Zn_xSb_2$,[53] $Ca_xYb_{1-x}Zn_2Sb_2$,[54] $Ca_5Al_2Sb_6$,[55] $BaGa_2Sb_2$,[56,57] etc.[58–63] In recent years our group has contributed significantly to the discovery and characterization of several other families of Zintl phases, including AE_2CdP_2,[64] Eu_3InAs_3,[65] $Ca_{14}AlBi_{11}$,[66] $Ca_{10}MSb_9$ (*M* = Ga, In, Mn, Zn),[67] $Ca_{9-x}RE_xCd_4Sb_9$,[68] $Ca_{10}RECdSb_9$,[69] among many others (*RE* = rare-earth metal).[70–76]

Besides the exploration of the Zintl phase materials for TE applications, an increasingly growing trend is the observation of topological properties of matter in a number of these phases.[77–80] Several known excellent TE materials are known to possess nontrivial topological properties as it appears both favor the same material properties such as strong spin orbit coupling (SOC) and narrow band gap.[46,81,82] Furthermore, it is known that several topological materials also exhibit some form of enhanced TE properties as strong correlations exists between the surface state properties of a topological material and transport properties such as *S*, σ and others, such that an enhanced TE performance can be achieved by tuning the surface properties.[83,84] It is important to also note that there is a growing interest in magnetism mediated TE properties through the incorporation of magnetic species in the material.[85,86] Moreso, such materials can provide a profitable playground to exploring exotic phases such as the higher order topology as found in $EuIn_2As_2$.[87] Aside from their prospect for understanding and developing excellent TE materials, TIs also hold great potential for spintronic applications.[88–90]

In this article, we will provide intuition into the correlated properties of TE materials and topological insulators (TI) and how such understanding can be exploited to develop new efficient TE generators. We will briefly cover the aspects of the physics of TI and thermoelectricity, followed by the chemist's perspective to TI and thermoelectricity. This will be followed by discussions of the contribution of bulk and boundary state properties of TI to thermoelectricity. In addition, discussions on selected Zintl phases are presented and how one can leverage their properties to develop high performance TE materials. We then conclude by providing a general outlook and perspectives on future research directions towards the development of efficient solid state thermoelectric generators. It is noted that aside from the Zintl phases, there are other classes of materials that have shown promises for TE applications which include the clathrates, skutterudites, half-Heusler phases, etc.[91–99]; they will not be discussed in this narrative as other articles have summarized their importance. We also wish to note that some aspects of the relationship between topological insulators and TE materials have already been dealt with in the literature.[81,82,100,101] Therefore, at the focus of this article will be on exploiting the close relationship between materials properties of TI and TE materials hosted by some newly discovered Zintl phases.

Topological Insulators (TIs) and Thermoelectrics (TE)

Topological insulators (TIs) are electronic material that behaves as ordinary electrical insulators (having an energy gap between the valence band and the conduction bands) in their bulk but with a gapless metallic state on their surface i.e., the valence and conduction bands are connected by metallic states known as edge or surface states.[102] These states can be attributed to the combined effects of strong spin-orbit coupling (SOC) and time-reversal symmetry and therefore TIs do not generally fall into the traditional Landau theory of phase transitions in matter.[103] In such a state, electrons of opposite spins (spin up and spin down) propagate in opposite directions (exhibiting helicity) in pairs with a spin-momentum locking and helps prevent the backscattering of electrons at their surface. Due to their robust surface states, they are protected against various time-reversal-invariant perturbations, such as scattering by impurities, surface deformation or distortion and crystalline defects.[104]

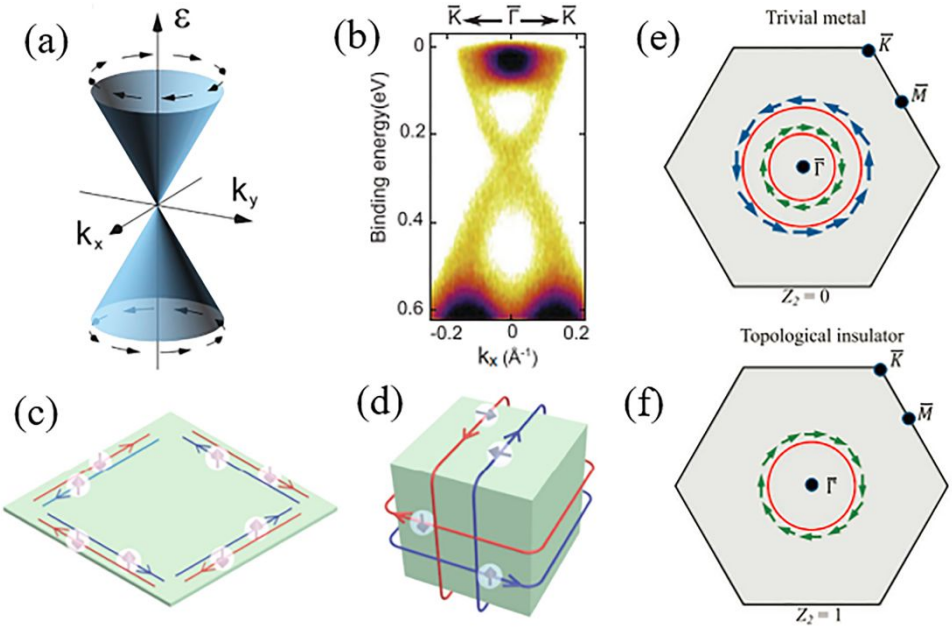

Figure 2. (a) The schematic representation of Dirac cones showing the energy spectra of topological surface states. The spin polarization is represented by the arrows. (b) Experimentally determined energy dispersion curve along high symmetry point for $GeBi_2Te_4$ based on reference 106 showing the Dirac cones formed. (c) and (d) are the schematic diagram of 1-D edge states of a 2-D TI and that of 2-D metallic surface states for a 3-D TI, respectively. The opposite moving electrons with opposite spins are denoted by blue and red lines. (e) and (f) The spin-polarized constant energy surfaces associated with the surface states of a TI and a trivial metal, respectively. Figure (a) is adapted from reference 100; Figure (b) is adapted from reference 106 with permission from American Physical Society, Figures (c) and (d) are adapted from reference 82 (CC BY), and (e) and (f) are adapted from reference 107.

Clearly, the profound difference between TIs and ordinary insulators (or trivial insulators) is the presence of gapless surface states with a linear dispersion in the former. In Figure 2(a), a simple illustration of the energy spectrum of the surface states of a TI is presented. The spectrum consists of two cones having a common vertex that are located in the energy gap between the bulk bands onto the surface band structure. Here, the spectrum is referred to as the Dirac cone while their touching point is the Dirac point. Also, the physics of relativistic Dirac fermions is relevant here since the nature of the surface dispersion results in a relativistic massless particles behavior of the surface Dirac fermions. The linear energy-momentum dispersion relationship of the fermions in these materials can be written as $E = pv$, with the speed of the massless particle v nearly two orders of magnitude slower than that of light in vacuum, thus, providing an opportunity of exploring the aspects of the physics of relativity in practical condensed matter systems.[105]

Since the observation of topological exotic state of matter in $Bi_{1-x}Sb_x$,[108] there has been several reports and predictions of such observation in a number of other narrow gap semiconductors.[109,110] Their characteristic fingerprints[111,112] includes strong SOC, a sign reversal of the molecular orbital symmetry, and an odd number of band inversion between the conduction and the valence bands. The odd number of band inversion implies that the number of Dirac cones in the surface band structure would be odd,[113] and as such several TE materials are also characterized by a Dirac cone situated around the Brillouin zone center Γ making them to have a nontrivial topology.[101] The relativistic effect and strong SOC characters in TIs are driven by their constituent heavy elements. On one hand, the relativistic effect elicits the lowering of the energy of the outer electrons of the 5s and 6s

orbitals while the strong SOC on the other hand triggers a band inversion and which can drive the realization of a non-trivial insulator state.[100,114,115] The strong SOC also lifts the spin degeneracy of the surface states and as well achieves the spin-momentum locking of the electrons. As shown in Figure 2(a), the electrons spin in Dirac states are oriented perpendicularly to the momentum while charge carriers with opposite momenta are aligned in an antiparallel fashion.[100]

In TE materials, the presence of heavy elements such as Sb, Te, Pb, and Bi with large atomic masses play a crucial role and are considered significant in driving low κ_L as found in PbTe[116] and Bi_2Te_3.[117] In bulk materials,[22] $\kappa\kappa_L$ can be determined as:

$$\kappa_L = 1/3 C_v V_g^2 \tau \quad (2)$$

where C_v, V_g, and τ are the specific heat, group velocity and phonon relaxation time. Hence, κ_L depends on these parameters and its magnitude can be effectively lowered via the minimization of τ, V_g, and C_v. A weak chemical bond and large atomic mass (due to heavy element) can drive the realization of a low V_g. It should also be noted that the coexistence of the presence of heavy elements and weak chemical bonds are ubiquitous in excellent TE materials.[118] The other aspect of reducing κ_L involves employing techniques of reducing the acoustic phonon such as intricate crystal structures, anharmonicity and introduction of point defects. Intuitively the aspect of the role-play of point defect in lowering the lattice thermal conductivity towards achieving an excellent TE performance is rooted in the surface state properties of TIs. Considering that the surface states of TIs are robust and protected against backscattering by nonmagnetic impurities, surface deformation and crystal structure defects, this feature inadvertently produces a TE material that satisfies "a phonon-glass-electron crystal" properties i.e., transport properties akin to that of a poor thermal conductor and a good electrical conductor.[13,119] By implication is would be possible to achieve significantly low lattice thermal conductivity while maintaining the high electrical conductivity on the topological surface states of TIs by simply creating a large number of defects. Hence, the nature of the surface states properties of TIs can provide for the decoupling of the phonon and electron transport towards designing efficient TE generators and coolers.[100] We note that such decoupling can lead to a significant change in the Lorentz number.

Chemists' perspective to TIs and TEs

The theoretical framework and description of TIs and thermoelectricity have been extensively studied and well established in condensed matter physics. However, the studies of these materials have received significant attention in recent years and have evolved into an interdisciplinary field of research involving condensed matter physics, materials science and solid-state chemistry. In addition, topology is a mathematical construct that deals with properties that are robust against small physical changes of the system. This implies that for a proper conceptualization of TIs, a body of knowledge that cuts across several fields and which provides for the classification of materials beyond just metal, semiconductor and insulators would be invaluable. While the physicists generally think in terms of bands and Fermi surface, the chemists tend to think in terms of molecular orbitals and bonding,[120] but this need not to be an issue as there has been previous works such as that of Prof. R. Hoffmann which provide a clear understanding into how the reasoning of physicist and solid state chemists meet in the understanding of the electronic properties of materials.[120,121]

Topological materials provide a fruitful playground for studies of exotic properties of matter, but the challenge lies in identifying suitable candidate materials that would permit for the experimental testing of the various theories. Chemists play a central role in the development and understanding of the various properties of both TI and TE materials. The first aspect of this relates to the materials synthesis and structural elucidation which involves materials design, exploratory synthesis, bonding optimization and most importantly the appropriate determination of the crystal symmetry and space group of these materials.[115,122,123] The classification of a material with either as trivial or non-trivial topology requires a good understanding of how the behavior of the electrons is intertwined with the symmetries of a material's crystal structure. Using the idea of topological quantum chemistry, a recent work has provided a classic topological classification of nearly all the reported inorganic materials by mapping the symmetry properties to coordinates in some high-dimensional space.[122] This provides for the prediction of materials with topological properties considering the type of atoms (with their atomic orbitals) located on a certain Wyckoff site in a given space group. The symmetry indicator developed from such technique provides a unique way of classifying materials as either metal, semimetal, insulating or topological.

In addition, the intuition of the solid state chemists which includes aspects of valence electrons "book-keeping", bonding requirements, atomic coordination numbers, etc. makes it possible to draw relevant structure-properties relationships, increase structural diversity, varying dimensionality and atomic bonding characteristics present in various materials.[123] Here we provide some simple clues to predicting and designing new TIs based on the general theoretical framework and features of known materials and later extend these ideas to Zintl TE materials. One of the first considerations to predicting if a material will be a TI relies on whether or not such material achieves a closed-shell electronic configuration according to simple electron counting using the Zintl-Klemm concept.[50] Generally, a bulk narrow band gap material is considered suitable for this purpose—a feature which is readily achievable in Zintl phases (*vide supra*). The second aspect involves the consideration of the presence of relativistic effect and strong SOC which are driven by the presence of heavy elements with large atomic masses. The SOC helps to achieve the inversion of the bands by impacting on the states close to the valence band maximum and the conduction band minimum. In addition, SOC could also achieve the task of band gap opening in semimetallic materials or those with a pseudo gap. Typically,

at least one of the heavy *p*-block elements such as Sb, Pb, Bi, etc., is required to satisfy this condition, which also provides for a *p*-character of the valence band and *s*-character for the conduction band. For example, it is assumed that in Zintl phases, that there is a complete transfer of electrons from the electropositive element to the electronegative elements. Therefore, the mixing of electronic state that is dominated by the electropositive element into the valence band and electronic states that is dominated by the electronegative element into the conduction band is of great importance. In materials where there are more than one *p*-block electronegative elements, such as in $MnBi_4Te_7$ and MBi_2Te_4 (*M* = Ge, Sn, Pb),[124,125] it is required that the differences in their electronegativities in the proximity of the conduction band minimum be as small as possible.[126]

Another important consideration to predicting the topological properties of a material relates to the crystal symmetry of the material, which requires the presence of an odd number of surface state bands crossing from the bulk valence band to the bulk conduction band over the whole Brillouin zone. In other words, the condition of an odd number of band inversion between the conduction and the valence bands must be satisfied.[113] As previously mentioned, several TE materials are also characterized by a single Dirac cone situated around the Brillouin zone center Γ making them to have a nontrivial topology.[127] Such feature can easily be achieved for a material with an axial symmetry for which, the conduction band minimum and valence band maximum are in the neighborhood of Γ. In general, it is conceived that the odd number of Dirac cones requirement can be achieved for a crystal system having a threefold symmetry, such as found in materials with *P*3 and *R*3 space group symmetries.[126] Beyond these general consideration, however, techniques of electronic structure calculations and experimental probes are necessary to unambiguously identify these materials. Such computational techniques would often involve electronic structure calculations of both the surface states and bulk band structures using suitable codes. Such an approach can be very powerful in unraveling the nature of the topology of the material, especially when combined with relevant theoretical framework such as parity analysis of occupied bands at the time-reversal invariant points in the Brillouin zone.[128,129] The various experimental probes serve the purpose of confirming or providing additional intuition into the various computational calculations and theoretical analysis. This involves the use of spin- and angle-resolved photoemission spectroscopy to unmask the presence of spin-polarized topological surface states as well as the visualization of the energy dispersion along the high symmetry points (See Figure 2(b)).[106] Similarly, other experimental techniques based on electrical and thermal transport properties measurements are also used to probe these materials and the reader is referred to other related articles such as in Ref. 115.

Next, we will consider the aspect of thermoelectricity from a chemist's perspective. Unlike TIs, the studies of TE have benefited significantly from chemists in every aspect as they are at the forefront of developing efficient solid state TE materials for both cooling and energy recovery purposes. The research themes in many solid-state chemistry labs that are focused on TE materials studies can involve the synthesis of single crystals, polycrystalline bulk samples, nanostructured materials, or the deposition of thin films. In addition, this area of research has also gained significant attraction among materials scientists and engineers who are mostly involved in the optimization of the properties through various techniques,[130,131] as well as device fabrications.[132,133] Several excellent TE materials are known to host nontrivial electronic topological features, as earlier indicated; as such, there is a strong correlation between excellent TE materials and TIs,[127,134–136] which buttresses the fact that they have similar material features. However, it should be noted that while most good TIs are excellent TE materials, the converse is not always true as in the case of $Yb_{14}MnSb_{11}$ and $Ca_9Zn_{4+x}Sb_9$.[51,52] This observation thus makes the prediction of excellent TE properties go beyond the presence of heavy element which can bring about the scattering of phonons towards lowering κ, as well as a narrow band gap that can promote the crossover of electrons from the valence band to the conduction band to promote a high σ. Other related consideration includes the presence of high valley degeneracy to promote high σ and phonon anharmonicity for low κ as well as low band effective mass (driven by the presence of strong SOC), high band degeneracy and resonant states among other.[130,137]

Generally, an effective way of achieving high performance of TE materials is through the decoupling of the electrical and thermal transport properties. This approach can further be achieved in TIs where the electronic and phonon transport can be effectively decoupled since the electronic transport is unaffected by backscattering from non-magnetic disorders and defects, which is at variance with the phonon transport. This approach thus allows for the independent tuning of $S^2\sigma$ and κ_L being the electronic and phonon contributions to *zT*, respectively. Similarly, another powerful parameter that can be invaluable to understanding the potential of these materials is the thermoelectric quality factor *B* [68,138] is defined as:

$$B=\left(\frac{k_B}{e}\right)\frac{8\pi e\left(2m_e k_B T\right)^{3/2}}{3\hbar^3}\frac{\mu_w}{\kappa_L}T=4.33\times10^{-10}\frac{\mu_w T^{5/2}}{\kappa_L} \quad (3)$$

where k_B, h, e, μ_w, and κ_L represent Boltzmann's constant, Planck constant, electronic charge, weighted mobility, and lattice thermal conductivity, respectively. It is immediately clear from this expression that $B \propto \mu_w/\kappa_L$, such that μ_w carries the same importance as κ_L and as such increasing the magnitude of μ_w is as important as achieving an ultra-low κ_L. By further expanding μ_w into its constituent parameters, this reveals that *B* is a function of the material's electronic and atomic structure and electron and phonon scattering,[139,140] as shown by the following expression:

$$B=\left(\frac{2k_B^2\hbar}{3\pi}\right)\left(\frac{C_l N_v}{m_l^* \Xi^2 \kappa_L}T\right) \quad (4)$$

where N_v is valley degeneracy, m_l^* is the inertial effective mass, Ξ is the deformation potential, and C_l is the average longitudinal elastic modulus. The various optimizations and doping to achieve these various conditions are ways towards the tuning of n to achieve an optimized zT.

Depending on the nature and degeneracy of the bands, there are established theoretical models such as the Single parabolic Band (SPB) or the Single Kane Band (SKB) models applied to parabolic and non-parabolic bands, respectively,[141–143] which can be used to predict the various aspects of a TE materials properties including the interdependence of the various transport parameters. Such models provide a good opportunity to make relevant predictions that can inform materials optimization and design. In recent times, there has also been the increasingly approach of various materials descriptors and machine learning approaches to predicting materials with potential for TE applications.[144–147] Such approach can provide for rapid materials screening and can be an invaluable way of selecting materials towards saving cost and time before embarking on elaborate experimental synthesis and measurements.

Contribution of topological insulators' bulk and boundary states to thermoelectric properties

The electronic structures of TI provide a vast window of opportunities to explore the various aspects of developing efficient TE generators and coolers based on various thermoelectric related effects such as Seebeck effect, magneto-Seebeck effect, Nernst effect, and Ettingshausen effect.[148] As earlier described, the electronic states of bulk and surface of a TI are different. The topological surface state in a 3-D TI is a 2-D surface, which covers the surface of the material, which can be conceptualized as a material with an electrically insulating interior, which is wrapped or coated with a thin layer of metal. Figure 2, panels (c) and (d), present the edge and surface states of 2-D and 3-D TIs. The aspect of the topological protected surface implies that if one tries to peel off the metallic layer of the material, the layer underneath then immediately becomes metallic. These surface states can be observed as Dirac cones in both computational and experimental results as shown in Figure 2 (a) and (b). In the early studies of TE materials, the contributions of the TI surface states were not taken into consideration. However, in recent times more research efforts have been directed towards the understanding of the role of the surface states in driving excellent TE properties. To this end, several theoretical and experimental results have emerged which provide for the contribution of the surface state to thermoelectricity.

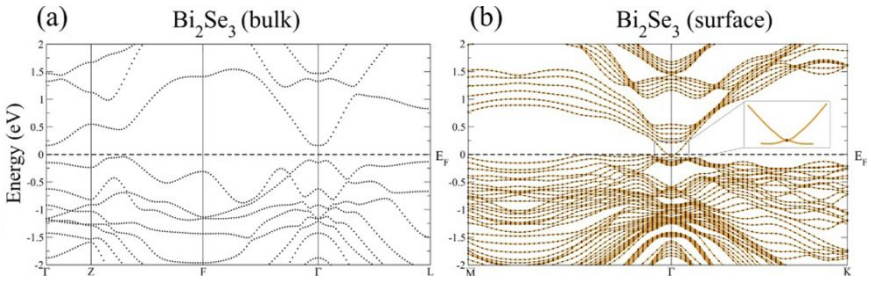

Figure 3. (a) The calculated bulk band structure of Bi_2Se_3 with spin-orbit coupling (SOC) and its (b) calculated surface state band structure of 5 quintuple layers of Bi_2Se_3 with a single Dirac cone. The Dirac cone formation is indicated in the inset. Figures adapted from Reference 81 (CCBY).

The study of the contribution of topological surface states to transport properties are often easily carried out on thin films or nanostructures.[149] It is noted that the contributions from edge and surface states to thermoelectric transport properties are geometric size dependent. We begin by considering the geometric dependent expression of zT given by:

$$zT=\frac{GS^2T}{K} \quad (5)$$

where $G = \sigma A/L$ is the electrical conductance, $K = \kappa A/L$ is the thermal conductance, based on the Ohm's and Fourier's scaling laws, respectively, within the diffusive transport regime.[150] The terms A and L are the cross-sectional area and length of the material, respectively, and it is obvious that the geometric factor A/L cancels out in the expression which shows the equivalence of Eqn (1) and (5) (*vide supra*) and showing that zT is independent of size. However, in TIs, the Seebeck coefficient S is size dependent, and the Ohm's and Fourier's scaling laws break down thus making zT size dependent. This effect can therefore drive the geometric dependent transport properties in these materials. For example, the relaxation time τ_s of the surface state in TIs is

much larger in comparison to that of the bulk state, which drives a significantly high surface state electrical conductivity σ_s. Another implication of the geometry dependence of the surface state of TIs is in its much longer mean free path, which gives rise to ballistic transport as opposed to the diffusive transport behavior of the bulk state. Based on the above, it is therefore obvious that surface states and bulk states would show different band structures as well as different transport properties. The band structure of the surface and bulk states of Bi_2Se_3 are shown in Figure 3 which portrays a significant difference between the two structures. The contribution of the surface and bulk states to thermoelectricity in TIs can be captured within the so called multiple-channel model. The Seebeck coefficient S can be expressed as a function of conductance G,[150] with the expression for a 3-D TI taking the forms:

$$G_T = G_b + G_s \quad (6)$$

$$S_T = (S_b G_b + S_s G_s)/G_T \quad (7)$$

where G_T, G_b, G_s, are the total, bulk, and surface conductance, respectively, while S_T, S_b, and S_s are the total, bulk, and surface Seebeck coefficient, respectively. It is noted that similar expressions can be written for a 2-D TI by replacing the terms for the surface states with those of edge states. In the above expressions, it is clear that both the surface and bulk states would contribute to thermoelectric transport properties wherein the Fermi energy E_F lies between the bulk and surface states. For a scenario where E_F is above the Dirac point and situated at the edge of the conduction band, $S_b < 0 < S_s$ and the contribution to S is weighted by G_b/G_s. Also under this scenario, the contribution of the surface states will often exceed that of the bulk.[148] Furthermore, it has been shown that even for diffusive transport (in 3-D TIs), the varying geometric factor could significantly impact on the relative contribution of both the surface and bulk states to S thus making zT size dependent in a TI.[151]

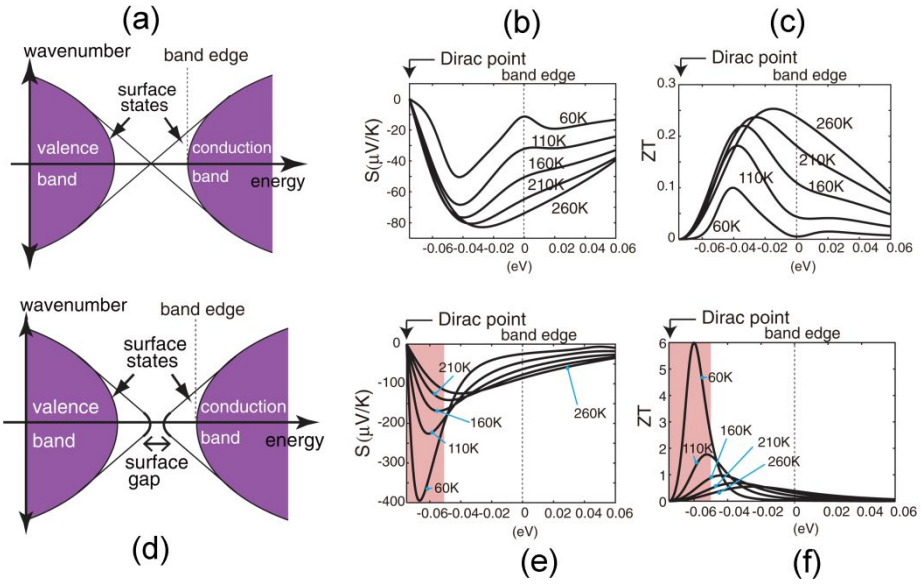

Figure 4. (a) A schematic diagram of the band structure of a 3D TI with the surface states. (b) and (c) are results from the electronic structure for Seebeck coefficient and zT as a function of the chemical potential, respectively. Similarly, (d) presents the schematic diagram of the 3-D TI band structure with the gapped surface states. (e) and (f) are calculated Seebeck coefficient and zT as a function of the chemical potential. Figures adapted with permission from reference 83.

The development of thin films provides an opportunity to study aspects of TI with and without hybridization effect in candidate TE materials.[152] In line with the multiple-channel model, studies have shown that, typical thin film developed from TIs without the hybridization effect can provide a robust conducting channel towards an improved TE property. In this regard, topologically protected surface states in TIs serve as conducting channels where by virtue of their low dimension show excellent transport properties in the absence of electron backscattering. It is therefore possible to completely tune the TE properties of such materials via the combination of geometric size control, lowering of phonon thermal conductivity through the introduction of defects and disorder, etc.

A schematic diagram of the band structure of a 3-D TI with gapless and gapped surface states are presented in Figure 4 based on the work from Ref. 83. Also shown are their respective calculated S and zT as a function of the chemical potential. In such calculations, the contributions of the respective surface states are incorporated and the presented S

and *zT* are from bulk and surface states. Here, it should be noted that the gapped 3-D TI is for a thin slab geometry model. The key highlight of this report indicates the presence of competing bulk and surface states transport such that the surface transport does not significantly contribute to the total electronic transport due to the effects of impurities. It is also evidence from these results that the transport properties of the gapped surface are much enhanced as compared to that of the gapless TI. The *zT* observed in the gapped system is relatively enhanced at low temperatures and for a gapped 3-D TI, *zT* is larger at low temperature when the chemical potential is in the proximity of the surface band gap. Such observation is akin to that of a narrow-gap material with a large *zT*, when the chemical potential is in the neighborhood of the gap. These results thus buttress the importance of thin film in the development of efficient TE materials.

Intuitions developed from some known and newly discovered Zintl phases

In the light of the various lines of discussions presented above, we proceed by discussing prospects of relevant Zintl phases with a view to provide a deeper understanding into how the properties of such materials can be harnessed for developing excellent TE materials.

The Sr_2X (*X* = Pb, Sn) and Ba_2X (*X* = Si, Ge) phases

We begin our discussion with the binary Sr_2X (*X* = Pb, Sn) and Ba_2X (*X* = Si, Ge) semiconducting Zintl phases. The Zintl M_2X (*M* = Mg, Ca, Sr, Ba; *X* = Si, Ge, Sn, Pb) Zintl phases[153–167] are reported to crystallize in a orthorhombic TiNiSi-type structure with the space group *Pnma* (No. 62).[153] The structure shown in Figure 5 (a) is a simple Cotunnite structure,[168] where the *M* atoms are found on two crystallographically inequivalent atomic sites. The first one has the *M* atom in a 5-coordinate geometry, while in the second one is bonded to four equivalent *M* atoms to form a mixture of corner and edge-sharing MX_4 tetrahedra. Conversely, some other members of the family such as the Mg_2Si (Mg_2Sn) crystallize with the face-centered-cubic antifluorite lattice type with space group $Fm\bar{3}m$ and is shown in Figure 5 (b). Detailed description of the aspects of the crystal structures of these phases have been reported.[156,169–171] These phases are rationalized as Zintl materials where the electropositive alkali earth metals donate their valence electrons to the group 14 *p*-block elements. As described earlier, these Zintl phases contain the basic ingredients required to drive a nontrivial TI state such as the presence of low band gap and heavy element as such there has been extensive studies on their topological properties.[172,173]

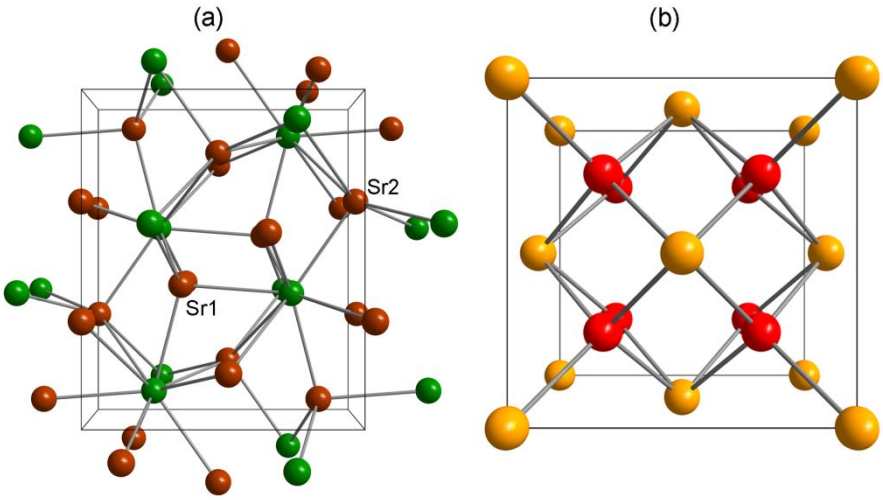

Figure 5. (a) Crystal structure of orthorhombic Sr_2Pb with the TiNiSi structure type, where the Sr and Pb atoms are shown brown and green spheres, respectively. (b) Crystal structure of cubic Mg_2Si. Mg and Si atoms are represented by red and yellow spheres, respectively.

The calculated band structures of Sr_2Pb with and without SOC effects are shown in Figure 6. The band structure in the absence of SOC, shows a metallic (gapless) character indicating that Sr_2Pb is not a TI in its native phase while the introduction of SOC opens a band gap of ~100 meV which is characteristic of a topological insulating state. In addition to the ordinary DFT calculations, results from hybrid Heyd-Scuseria-Ernzerhof (HSE)[174] also confirms this observation with a much larger band gap. This phase lies in the proximity of a topological instability and can be carefully tuned with a uniaxial strain. Such consideration and application of strain along the *ac* plane (the 010 surface) which is synonymous to probing a thin film as a function of its thickness. In Figure 6 (e) and (f), the band structure from such calculation is presented and indicates the viability of driving the phase into a TI with a relatively small uniaxial strain that exceeds 3 %. It is also noted that other

members of this family, such as Ba_2Si and Ba_2Ge,[173] have also been identified as hosting a topological semimetal phase with a nodal ring in the $k_x = 0$ plane, that is protected by the glide mirror symmetry in the absence of SOC. These phases also present key examples of tuning the topological state through the application of an elastic strain. Key features in the electronic band structure of these phases that achieve a TI state are thought to be amenable towards driving excellent TE properties in several of them. Theoretical calculations[175,176] reveal their potential for TE applications.

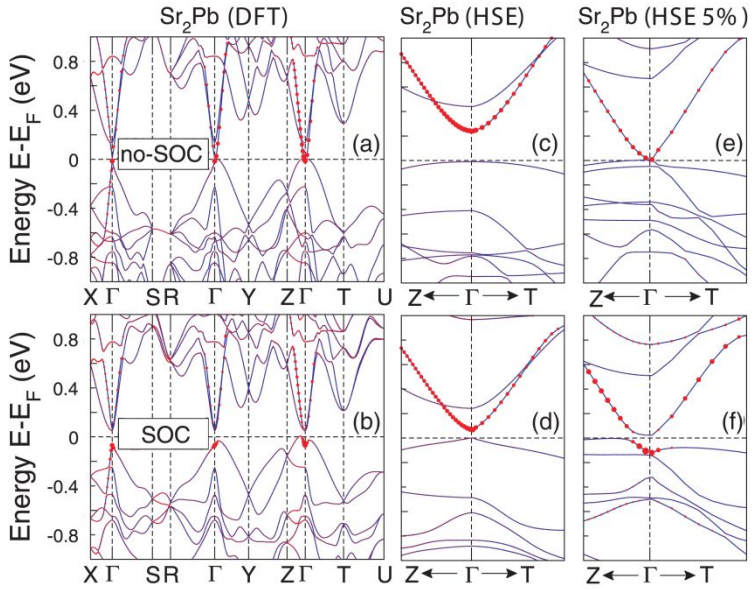

Figure 6. DFT-calculated electronic band structures of Sr_2Pb without (a) and with SOC (b) under consideration. HSE band structures around the point along the Z-T directions for Sr_2Pb. (c) and (d) are the electronic band structure at zero strain while (e) and (f) are the band structure under 5% tensile strain in the ac plane. The solid symbol represents states with a predominant *s*-like character. Figure adapted from reference 172, with permission from the American Physical Society.

Consider the band structure of all Ca_2Pb, Sr_2Pb and Ba_2Pb presented in Figure 7 (a) to (c) with estimated direct band gaps of 0.33, 0.38 and 0.18 eV, respectively. The effect of strong SOC is important in these phases as driven by the large atomic mass of Pb. An important aspect of these materials is their anisotropic valence band structure wherein the slope near the VBM is observed to vary nearly by a factor of 5 in a specific direction. Such observation will also impact on the carrier mobility and will thus play a crucial role in their TE transport properties and performance. Also, the conduction bands of Ca_2Pb and Sr_2Pb indicate a near-degeneracy, involving two maxima, which can be beneficial for the TE transport properties. It is further noted that the calculated density of states (DOS) near the Fermi level shows rapid increase, which thus provides for a small energy scale and enhanced Sebeck coefficient. It is also worth mentioning that the relatively small band gap observed in Ba_2Pb would likely give rise to a bipolar conduction, which can prove to be detrimental to the high temperature TE performance. The Ba_2Pb phase will therefore be more promising in the moderate temperature regime and for applications as solid-state coolers. An additional intuition into the transport properties of these phases is provided via their Pisarenko plots, shown in Figure 7 (d) to (f). In Ca_2Pb, the optimal doping for TE performance at 300 K is between 4×10^{18}–1.5×10^{19} cm^{-3}. At 500 K and 800 K, the detrimental effect of bipolar conduction is likely to be at play but can be overcome via appropriate doping. It should be noted that a significantly high magnitude of Seebeck coefficient that exceeds 200 $\mu V\ K^{-1}$ can be realized under optimal doping despite the narrow band gap thus arguing in support of their promising high temperature TE performance at 1000 K.

In Sr_2Pb, a gradual transition into a degenerate behavior as the carrier concentrations increases is observed. Similarly, the bipolar regime only sets in near 800 K at optimal doping for the *p*-type material while for a *n*-type, a promising performance is predicted at 800 and 1000 K. As earlier noted, the likelihood of a bipolar conduction at elevated temperature in Ba_2Pb is high and which is consistent with the relatively small Seebeck coefficient of ~200 $\mu V\ K^{-1}$ for *p*-type at 800 K. The Ba_2Pb phase being the heaviest however presents an advantage of having the lowest lattice thermal conductivity as unraveled from the calculated low bulk moduli that is much smaller than those observed in well studied lead chalcogenides,[177] thus making it more suitable for room temperature or moderate temperature applications.[175] The Ca and Sr phases on the other hand are projected for high

temperature applications which is supported by high temperature electrical conductivity.

We conclude this section by discussing the features of the isostructural stanides phases, Ca_2Sn, Sr_2Sn and Ba_2Sn. These phases are reported to have larger band gaps and higher lattice thermal conductivity. The remarkable aspect of these materials is their high Seebeck coefficient that exceeds those of the plumbides and which is attributed to their wider band gaps. These materials class thus presents a viable playground to explore new high performance TE materials that can be deployed for various solid-state applications. It is reported that several of these phases are congruently melting and as such should provide us with a great opportunity of synthesizing the various phases towards investigating their transport properties and various optimization techniques.[156,176–179] Despite the promising TE transport properties that can be explored in these phases, there are only a handful of experimental results on these materials. We note that the first reported experimental result on Ca_2Pb was carried out over 6 decades ago by Russell and Klein where they observed a room-temperature zT of about 0.2 in Ca_2Pb,[182] which is consistent with the features described based on electronic structure calculations. However, such an interesting result has not been probed further. Efforts towards high temperature probe of these materials and materials optimization are therefore expected to provide an invaluable insight into their excellent TE properties. Another interesting results on the cubic Mg_2X (X = Si, Ge, Sn) and some of their quasi-binary alloys have been reported[183,184] with the optimized composition $Mg_2Si_{1-x}Sn_x$ resulting in a remarkable zT = 1.1 near 800 K. Furthermore, several works geared towards optimization of the TE performance have yielded remarkable results.[185–194]

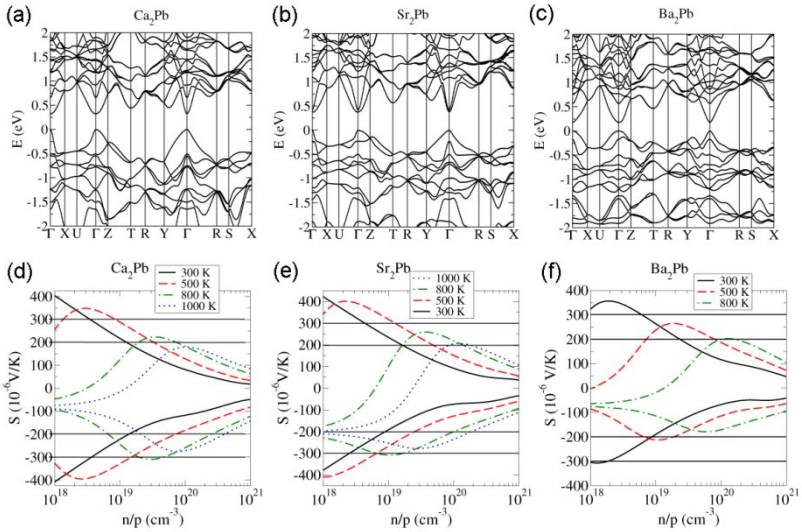

Figure 7. The band structures of Ca_2Pb, Sr_2Pb and Ba_2Pb, within the orthorhombic Brillouin zone are shown in (a), (b), and (c), respectively. Conductivity weighted Seebeck coefficient of (d) Ca_2Pb, (e) Sr_2Pb, and (f) Ba_2Pb where the horizontal lines demarcate the region of Seebeck coefficient absolute value between 200 and 300 μV K^{-1} being the ideal range for a high-performance TE. Figures adapted from reference 175 (CC BY-NC-SA 3.0).

The AIn$_2$As$_2$ (A = Ca, Sr, Ba and Eu) Zintl phases

Next, we have chosen to highlight the features of the AIn$_2$As$_2$ (A = Ca, Sr, Ba, Eu) Zintl phases. The crystal structure of CaIn$_2$As$_2$ and BaIn$_2$As$_2$ are schematically presented in Figure 8. The BaIn$_2$As$_2$ phase has the monoclinic EuGa$_2$P$_2$ structure type,[195] while the AIn$_2$As$_2$ (A = Ca, Sr, Eu) phases have a layered centrosymmetric hexagonal structure (space group $P6_3/mmc$); the latter belongs to a class of materials that have recently been studied for their topological properties.[46,196,197] The hexagonal EuIn$_2$As$_2$[196] phase undergoes an A-type anti-ferromagnetic (AFM) ordering at T_N = 17 K, and shows a colossal magnetoresistance (CMR) of magnitude −143 % at 17.5 K and in an applied field of 5 T. Similar observations are reported in EuIn$_2$P$_2$[198] with T_N = 24 K and CMR of −298 % at 24 K and in an applied field of 5 T. The EuIn$_2$As$_2$ phase is a magnetic topological insulator with an estimated band gap, E_g = 0.1 eV along the Γ-M direction, and where the Eu^{2+} electronic state of $4f^7$ is localized. Depending on the orientation of the magnetic moments, the A-type AFM order in EuIn$_2$As$_2$ can lead to either an axion insulator (magnetic TI in which the nontrivial $\mathbb{Z}_2$ index is protected by inversion symmetry instead of time-reversal symmetry)[199] or a higher-order topological insulator with chiral states existing on the hinges between the gapped surfaces.[87] Similarly, the CaIn$_2$As$_2$ and SrIn$_2$As$_2$ phases have been reported as TIs.[46,197] Although, the experimental transport properties are yet to be reported, results from electronic structure calculation show that these phase holds some promise with enhanced TE properties. A key drawback here, however, would be the presence of As

element in the phase which could pose serious health challenges. It is therefore expected that phases where the As is replaced by a much heavier Sb would be more suitable in this regards as demonstrated in recent theoretical calculations.[200] Such calculations in fact reveal that a $zT > 1$ can be achieve in $CaIn_2Sb_2$ and $SrIn_2Sb_2$ at moderate temperatures (See Figure 9) which can find applications as Peltier coolers. An important aspect of these results is the calculated low lattice thermal conductivity, which is beneficial for developing efficient TE materials. To our knowledge, the successful synthesis of the phases AIn_2Pn_2 (A = Ca–Ba, Eu; Pn = Sb, Bi) has not been reported to date. This may have to do with "competition" from other thermodynamically stable phases in the respective systems, and as such, one would have to depend on synthetic chemists to figure out the relevant conducive environment and methods to grow crystals of these materials with potentially very interesting properties.

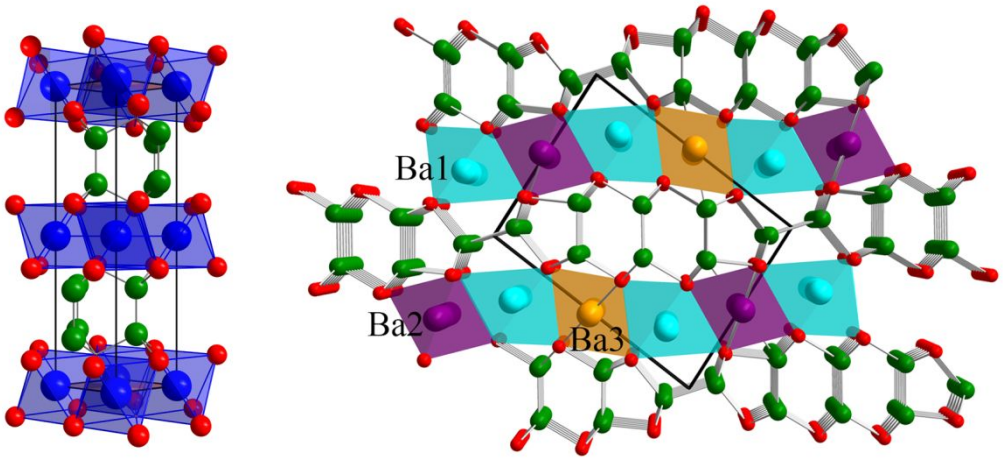

Figure 8. (a) Crystal structure of $CaIn_2As_2$ with the layered arrangements of the atoms emphasized and only the In–As bonds are drawn, for clarity. (b) Crystal structure of $BaIn_2As_2$ structure. The unit cells are marked out by the solid (black) line.

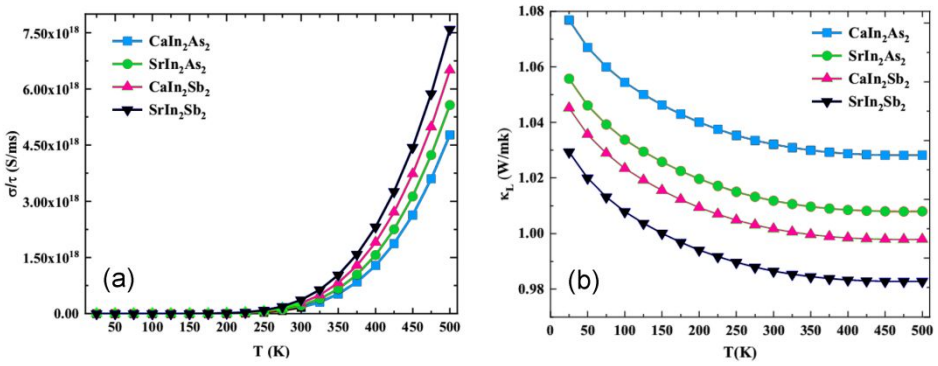

Figure 9. (a) Calculated temperature dependence of electrical conductivity of AIn_2Pn_2 (A = Ca, Sr and Pn = As, Sb). (b) Calculated temperature dependence of lattice thermal conductivity of AIn_2Pn_2 (A = Ca, Sr and Pn = As, Sb). Figures redrawn with data from reference 200.

Other reported isostructural compounds that are of interest are $CaIn_2P_2$ and $SrIn_2P_2$ phases.[201,202] Both compounds are narrow gap semiconductors with $CaIn_2P_2$ and $SrIn_2As_2$ having an indirect $E_g = 0.39$ eV and a direct $E_g = 0.28$ eV, respectively.[203] Furthermore, a quantum phase transition from a semiconductor to a nontrivial topological phase is reported in both compounds, where the application of a minimal strain leads to a band inversion and the subsequent opening of a band gap along the line node in the presence of SOC.[204,205]

The $YbMnSb_2$, $EuZnSb_2$, and $AAgPn$ (A = Ca, Sr, Ba; Pn = Sb, Bi) phases

The Zintl phases $YbMnSb_2$[206] and $EuZnSb_2$[207] are topological Dirac semimetals (TDSM), which similarly to TIs have in their bulk band structures an inverted order of the occupied valence and unoccupied conduction bands at the time-reversal invariant momenta (TRIM) in the Brillouin zone (BZ). However, as opposed to TIs (*vide supra*), the band inversion in TDSMs is characterized by a two-dimensional topological invariant, $\nu_{2D} = 1$ which results in the appearance of Dirac cones already

in the bulk and which is protected by crystalline symmetries.[208] The crystal structure of $YbMnSb_2$ and the depiction of bands in a TDSM are shown in Fig. 10 (a) and (b), respectively. Previous reports on the $YbMnSb_2$ phase reveal the presence of quantum oscillations, which provide the transport evidence for the existence of Dirac fermions. Such quantum materials provide an additional fertile playground to explore the various aspects of exotic electronic structures that may be relevant in various application areas. In particular, the nature of their Fermi surface and intricate band structures can directly influence the realization of excellent TE properties. As in the case of TI, the contribution of the Dirac bands to the overall TE performance through the combined effect of enhancement of S and σ can be explored. This line of thought was recently established in the studies of $YbMnSb_2$,[209] where the material although being a semimetal exhibits a significantly large magnitude of S (160 μV K^{-1}) both along the dispersive and non-dispersive directions at 300 K and which is further accompanied by a low lattice thermal conductivity (1 W m^{-1} K^{-1}) and a low electrical resistivity along the highly dispersive direction.

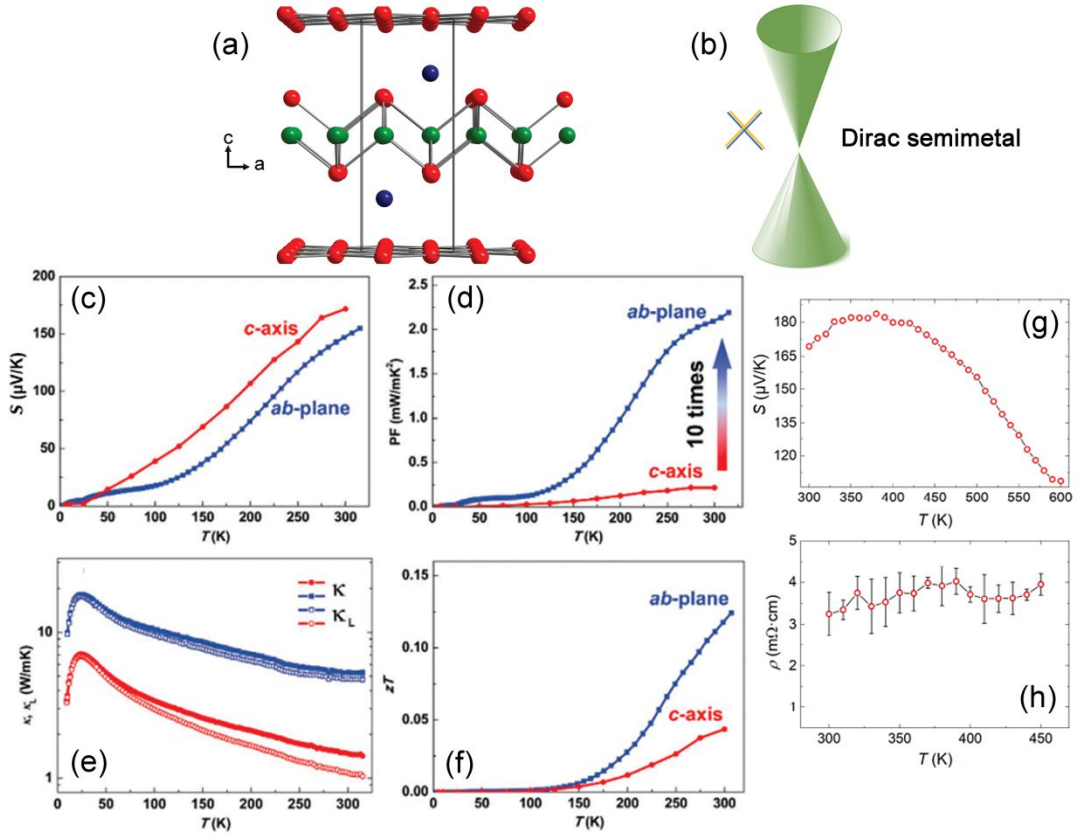

Figure 10. (a) Schematic crystal structure of $YbMnSb_2$ phase, viewed along the *b*-crystallographic direction. The Yb, Mn and Sb atoms are represented by blue, green and red spheres, respectively. Schematic depiction of bands in a Dirac semimetal. (c): The Seebeck coefficient, (d): thermoelectric power factor, (e) total and lattice thermal conductivity, (f), and zT of $YbMnSb_2$ reported by Pan et al.[209] below room temperature (g) Seebeck coefficient, and (h) electrical resistivity of $YbMnSb_2$ reported by Baranets and Bobev[206] above room temperature. Figures (c) to (f) are adapted from reference 209 (CC BY 4.0) and Figures (g) and (h) are adapted with permission from reference 206.

In Figure 10, key promising results on $YbMnSb_2$ are captured and reveal the role-play of the highly dispersive Dirac and regular bands in achieving an enhanced TE power factor. Here it is noted that the observed power factor at 300 K and the average sound velocity υ_s (1990 m/s) are superior when compared to those of the state-of-the-art tetradymite.[210,211] These results thus argue in favor of the potential of exploring such novel semimetals in designing highly efficient TE generators. For example, the observed room temperature zT of 0.12 along the *ab*-plane can be significantly improved through a number of techniques directed towards achieving ultra-low lattice thermal conductivity and further enhancement of the TE power factor. It is further noted that in the high-temperature regime, available data suggests the manifestation of a bipolar effect, which is ubiquitous in semimetals with characteristic small S by virtue of the conduction of two types of charge carriers. Fig. 10 (g) shows S in the temperature range of 300 K and 600 K.[206] The magnitude at room temperature is fairly reconcilable with the low-temperature report by Pan et al (Fig. 10 (c)),[209] and shows

an increase to about 380 K with a magnitude of ~180 μV K^{-1} before the detrimental bipolar conduction effect sets in with a resultant decrease in *S* to 109 μV K^{-1} at 600 K. Such observation likely portrays $YbMnSb_2$ as a candidate TE material in the moderate temperature range, i.e., its properties can be harnessed for TE cooling. It also suffices to note that the dispersive degenerate bands with an attendant larger regular band that accompanies TDSMs can pave a new pathway to taking advantage of these materials to achieving efficient TE generators. By such, it may be possible to circumvent the disadvantage bipolar effect by suppressing the excitation of the minority charge carriers.

As earlier indicated $EuZnSb_2$ is also a TDSM,[207] and along with other related phases[212–215] presents a fruitful playground to explore the influence of complex band structure and Dirac bands to achieving excellent TE performance. It, therefore, remains to be seen how the robust electronic band structure of the various phases will play out as it pertains to the evolution of their respective TE transport properties.

Finally, we proceed to examine the hexagonal *A*Ag*Pn* (*A* = Ca, Sr, Ba; *Pn* = Sb, Bi),[216,217] wherein the observation of TDSM state is prevalent.[218–221] A key aspect of these materials, which can be described as Zintl phases with coinage metals, is their low lattice thermal conductivity that drives their excellent TE properties.[222,223] For example, studies on the CaAgSb phase with the TiNiSi-type[224] indicate a transition into the LiGaGe-type phase[225] upon substituting some of Ag for Zn to give $CaAg_xZn_{(1-x)/2}Sb$ with attendant ultralow lattice thermal conductivity of (~0.4 W m^{-1} K^{-1}) for $CaAg_{0.2}Zn_{0.4}Sb$ between 300 K to 773 K.[226] The results further indicate the presence of an all-scale hierarchical structure that supports effective phonons scattering over a wide frequency range. This observation along with other features such as twin boundary, nanoprecipitate, atomic site vacancy, etc. are attributed to driving the observed ultra-low lattice thermal conductivity which is much improved when compared to the parent CaAgSb phase. Another important aspect of these results relates to the enhancement of *S* upon the transformation from CaAgSb to $CaAg_{0.2}Zn_{0.4}Sb$ by over a factor of 3 which together with the realized ultra-low lattice thermal conductivity results in a *zT* ~0.8 at 773 K. Similar studies on $Ca_{1-x}RE_xAg_{1-y}Sb$ (*RE* = La–Nd, Sm) with the LiGaGe-type was also reported to exhibit enhanced *zT* at elevated temperatures.[227] Here, the optimized composition of $Ca_{0.84}Ce_{0.16}Ag_{0.87}Sb$ produced a *zT*~0.7 at 1079 K.

Furthermore, several other reports exist on the demonstration of the promising TE properties in the equiatomic *A*Ag*Pn* family including those of SrAgSb,[61] SrAgBi,[228] BaAgSb,[229,230] BaAgBi,[231] BaAgAs,[232] and related phases.[222,233,234] The various results demonstrate the robustness of these quantum materials to hosting excellent TE properties. While a number of reports already exist on the excellent TE properties harbored by this family of materials, it is noted that a number of them are yet to be properly investigated and it is at the heart of this article to draw close attention to such promising materials. In specific terms, these materials present a window of opportunity to accessing the "phonon-glass-electron crystal" properties,[13,119] which provide for ultra-low lattice thermal conductivity and high TE power factor. As such the realization of interesting TE transport properties in the various phases is driven by the amenability of the phases to effective decoupling of the phonon and electron transport. In this wise, akin to the similar material properties between TIs and TE materials, TDSMs also present us with ample opportunity to taking advantage of the nature of their Fermi surface and intricate band structure to engineer high-performance TE materials that can find applications in various areas either as solid state cooling or for power generation.

The *AXPn* (*A* = alkali metal, *X* = divalent metal; *Pn* = pnictogen) phases

The equiatomic Zintl *AXPn* phases (*A* = Na, *X* = alkaline-earth metal) are ternary derivatives of the 3-D topological Dirac semimetal Na_3Bi, which has attracted much attention due to its interesting physics.[235–237] Although structurally not identical, NaBaBi can be conceptually formed by way of replacing two monovalent Na atoms with a divalent Ba atom. This analogy can be extended to the other alkaline-earth metals, including the nominally divalent rare-earths Eu and Yb, which potentially creates a large class of interesting materials. The NaBaBi and its analogous phases crystallize in the non-centrosymmetric hexagonal $P\bar{6}2m$ space group (# 189) while Na_3Bi has a centrosymmetric structure with the hexagonal $P6_3/mmc$ space group (# 194). NaBaBi is reported as a TI under pressure that breaks the inversion symmetry observed in Na_3Bi.[238] Similarly, features of strong TI have been observed in NaCaBi and KBaBi where band inversions under strong SOC are evidenced.[239] It is also noted that similar observations have been reported in other related KZn*Pn* phases.[240] Just very recently, a number of new phases namely NaSrSb, NaBaSb, and NaEuSb have been reported by our group,[241] which further provides for ample opportunities to probe the rich electronic structures and properties harbored by these class of materials. Preliminary electronic structure calculations reveal features akin to supporting the formation of Dirac states. The band structures of NaSrSb and NaBaSb are presented in Figure 11 and it is expected that their topological properties could be properly tuned with the inclusion of SOC and strain effect which are considered essential ingredients that drives the realization of topological phases in condensed matter. The electronic band structures shown in Figure 11 have been computed using the TB-LMTO-ASA code,[242] with the local density approximation, and the reader is referred to Ref. 241 for additional details. It is noted, however, that the LMTO-predicted band gap is overestimated, and that it is expected subsequent studies to provide more accurate estimation of the band gaps. For the desired accuracy, such follow-up work must employ hybrid functionals such as the Heyd, Scuseria and Ernzerhof (HSE)[174, 243].

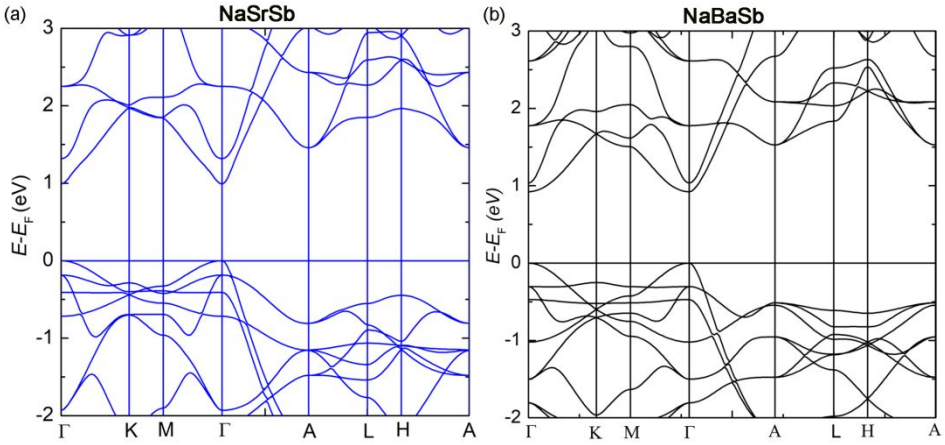

Figure 11. (a) Electronic band structure of (a) NaSrSb and (b) NaBaSb in the absence of spin-orbit coupling effect. Figures are produced with permission from Reference 241.

In line with the propensity of topological materials to promote excellent TE properties, literature available reveals that there are very sketchy probes into the aspects of the thermoelectricity of these phases as potential TE materials. However, the available report indicates that the electronic and phononic features in NaBaBi could exhibit excellent TE properties for both the *n*- and *p*-type materials and can be explored as candidate TE coolers.[244] The results predicted a cross-plane and in-plane $zT \sim 2$ and ~1, respectively, at 300 K for both charge carrier types. With further temperature rise, the magnitude of zT approaches a significant value of ~2.5 for the *p*-type materials. However, for the isotropic scenario, reduced values of ~1.2 and 1.6 are predicted for the n- and p-type materials. The observed features here are thought to be driven by its low DOS and highly non-parabolic bands that promote high σ and S, respectively, which coupled with strong phonon anharmonicity are beneficial for TE properties. Reports on LiBaSb on the other hand predict it to have an indirect band gap and with lower TE merit in the temperature range of 300 K to 350 K where NaBaBi tends to possess an optimal performance. Features from the calculations in fact reveal that LiBaSb achieves a $zT \sim 0.6$ at 500 K with monotonically increasing features toward higher temperatures. With no sign of bipolar conduction, it could be inferred that at much elevated temperatures, this phase could approach a $zT \sim 1$. It is noted that the LiBaSb shows an energy band gap of ~0.8 eV which is comparable to the value of ~0.9 eV in NaSrSb and NaBaSb showed in Figure 11, the difference being that the Na phases are direct band gap materials similar to that of NaBaBi and are expected to also show promising TE behavior.

While theoretical calculations on these phases show interesting topological properties and promises for TE applications, experimental results to both verify and explore other properties of interest are still lacking. Against the backdrop of this is the relative difficulty in synthesizing sizable single crystals or polycrystals that would allow for their exhaustive investigations. With the successful synthesis of NaSrSb, NaBaSb, and NaEuSb, we hope to develop an optimized synthesis approach to accessing the various related phases that would provide us with a rich material landscape for studying their topological, thermoelectric and other emerging properties.

General outlook and conclusions

In this brief review article, we have taken a cursory look at the chemist's conceptualization and contributions to our understanding of TIs and thermoelectricity, which are known to have related material properties. Particularly, we looked at the aspect of the contribution of boundary states to thermoelectricity and how such could help develop new highly efficient thermoelectric materials. Such development is currently at the forefront of scientific intervention of mitigating the adverse effect of greenhouse gasses on the environment as well as addressing the world's energy crisis through alternative clean source of energy in the form of solid-state thermoelectric coolers and recovery of waste heat into reusable form.

We also evaluate the various features of the surface state of a TI that may be beneficial for achieving enhanced TE properties such as its protection against backscattering by nonmagnetic impurities, surface deformation and crystal structure defects. We considered that such feature can be used to engineer a TE material that satisfies the desired "phonon-glass-electron crystal" properties,[13,119] which can provide for a window of opportunity of driving a significantly low lattice thermal conductivity while simultaneously maintaining a high electrical conductivity on sample material. It is thus plausible to consider such decoupling of the phonon and electron transport as a viable way of designing efficient TE materials. Furthermore, a defining feature of TIs is the presence of odd number of Dirac cones situated around the Brillouin zone center Γ making them to have a nontrivial topology,[101] and it is noted that known TIs with remarkable TE properties has one Dirac cone at the Brillouin zone center. It

would therefore be of interest to observe how the presence of three or five Dirac cones will impact on the TE properties.

It is further noted that although known TIs are good TE materials, the converse is not always true as there are a number of materials with excellent TE properties, but which exhibit trivial topology. We therefore also considered the various aspects of techniques employed in optimization of TE properties, which includes band convergence, weak chemical bond, structural complexity, interstitial defects, presence of elements with a large atomic mass, etc. An effective way of tuning candidate material involves decoupling the materials properties into electronic and phonon contribution part with the electronic part given by the TE power factor $S^2\sigma$ and the phonon part by κ_L.

We thus conclude by discussing a number of Zintl TIs so as to provide contest into our discussions on how to harness the characteristic feature of TIs for developing efficient TE material. One of such examples are the binary Zintl phases Sr_2X (X = Pb, Sn) and Ba_2X (X = Si, Ge), where extensive electronic calculations and preliminary experimental measurements provide support for the presence of excellent TE properties in them. An important aspect of the presented results includes theoretical calculations that consider the contributions of surface and bulk transport to the total TE properties. The key highlight of this report indicates the presence of competing bulk and boundary states transport where it was observed that the surface transport does not significantly impact on the total electronic transport due to the effects of impurities. However, in gapped TIs (thin slab), the calculated zT was found to be much enhanced at low temperature when the chemical potential is in close to the surface band gap. Such observation thus argues in support of the need to grow thin films of relevant materials on appropriate substrates towards the development of highly efficient TE material.

We also highlighted the AIn_2Pn_2 (A = Ca, Sr, Ba, Eu; Pn = P, Sb, Bi), where we presented results of some theoretical studies on $CaIn_2Sb_2$ and $SrIn_2As_2$ which shows excellent TE properties. While the various phosphide and arsenide phases have been synthesized, those of antimonides and bismuthides are yet to be synthesized. However, in view of the presented electronic structure calculation, which also predict the phase stability of such phases, it is expected that concerted effort would be put in place by solid state synthetic chemists towards the preparation of such phases which will then allow for the experimental investigation and verification of the various transport properties calculations. In the same vein, we discussed the various aspects of materials design of TIs and thermoelectricity, which can be invaluable in the development of new materials with specific characteristic features.

At the very heart of the various discussions and materials considerations is the exploratory materials synthesis, which has continued to fuel research activities both from the fundamental and applied fields of science and engineering perspectives. The synthesis of new and diverse solid state materials would therefore further avail us the opportunity and playground to both test the various theories of physics and channel a pathway of optimizing the various material properties. While we have briefly examined the interrelationships between TIs and thermoelectrics on some recently developed Zintl phases, progress in the development of new and innovative synthetic techniques would be invaluable in accessing several other phases that may be of great benefit and interest. Furthermore, more robust theoretical and computational models are expected to help us directly correlate the topological properties of the various materials to their TE performance while taking the surface state properties into consideration. Such success will no doubt promote the rapid development of efficient TE materials but will also help to save time and resources expended on some dead-end measurements. In recent times, the deployment of machine learning algorithms in the studies of condensed matter systems and in the prediction of material properties has been on the rise. The development of machine learning tools that would further facilitate the screening of materials and one that takes into cognizance their topological properties to predict TE properties would be pivotal to accelerating the development of an emerging class of TE materials. Going by the need to develop efficient TE coolers and generators that can strategically be deployed to mitigate the devastating impact of the emission of greenhouse gases, highly efficient and stable TE materials with $zT > 1$ are needed. In recent times, the conversations have even now shifted from achieving $zT > 1$ to those of super-thermoelectric materials with $zT > 5$.[245] While achieving such zT magnitude in a practical material seems like a daunting task, progress in the synthesis of new materials and development of powerful predictive tools would be key to driving such possibilities.

Author contributions

The manuscript was written through contributions of all authors. All authors have given approval to the final version of the manuscript.

Conflicts of interest

There are no conflicts to declare.

Acknowledgements

Own work cited in this review article was supported by the U.S. Department of Energy, Office of Science, Basic Energy Sciences through grant DE-SC0008885.

Notes and references

1 United nations Climate Change Press Release, Climate Plans Remain Insufficient: More Ambitious Action Needed Now, 2022.
2 N. Ma, J. H. Jiang, K. Hou, Y. Lin, T. Vu, P. E. Rosen, Y. Gu and K. A. Fahy, Earth Sp. Sci., , DOI:10.1029/2022EA002662.
3 Intergovernmental Panel on Climate Change (IPCC) Report, The evidence is clear: the time for action is now. We can halve emissions by 2030, 2022.
4 J. Meckling, T. Sterner and G. Wagner, Nat. Energy, 2017, **2**, 918–922.
5 S. Patidar, Int. J. Res. Appl. Sci. Eng. Technol., 2018, **6**, 1992–1996.
6 S. Riffat and X. Ma, Appl. Therm. Eng., 2003, **23**, 913–935.
7 J. Mao, G. Chen and Z. Ren, Nat. Mater., 2021, **20**, 454–461.

8 I. Petsagkourakis, K. Tybrandt, X. Crispin, I. Ohkubo, N. Satoh and T. Mori, Sci. Technol. Adv. Mater., 2018, **19**, 836–862.
9 Y. Dong, M. Coleman and S. A. Miller, Annu. Rev. Environ. Resour., 2021, **46**, 59–83.
10 B. K. Sovacool, M. Bazilian, S. Griffiths, J. Kim, A. Foley and D. Rooney, Renew. Sustain. Energy Rev., 2021, **143**, 110856.
11 C. Aprea, A. Greco, A. Maiorino and C. Masselli, Int. J. Heat Technol., 2018, **36**, 1155–1162.
12 D. Zhao and G. Tan, Appl. Therm. Eng., 2014, **66**, 15–24.
13 G. S. Nolas, D. T. Morelli and T. M. Tritt, Annu. Rev. Mater. Sci., 1999, **29**, 89–116.
14 A. Saini, R. Kumar and R. Kumar, in Thermoelectricity and Advanced Thermoelectric Materials, Elsevier, 2021, pp. 1–19.
15 T. J. Seebeck, Magnetische polarisation der metalle und erze durch temperatur-differenz, W. Engelmann, 1895.
16 J. C. Peltier, Ann. Chim. Phys., 1834, **56**, 371–386.
17 A. v. Ettingshausen and W. Nernst, Ann. der Phys. und Chemie, 1886, **265**, 343–347.
18 H. Adachi, K. Uchida, E. Saitoh and S. Maekawa, Reports Prog. Phys., 2013, **76**, 036501.
19 G. J. Snyder and E. S. Toberer, Nat. Mater., 2008, **7**, 105–114.
20 M. O. Ogunbunmi, S. Baranets and S. Bobev, Chem. Mater., 2021, **33**, 9382–9392.
21 T. M. Tritt, in Encyclopedia of Materials: Science and Technology, Elsevier, 2002, pp. 1–11.
22 C. Kittel, Introduction to Solid State Physics, Wiley, new York, 8th edn., 2018.
23 J. R. Sootsman, D. Y. Chung and M. G. Kanatzidis, Angew. Chemie Int. Ed., 2009, **48**, 8616–8639.
24 Y. Ouyang, Z. Zhang, D. Li, J. Chen and G. Zhang, Ann. Phys., 2019, **531**, 1800437.
25 P. Wei, C. Liao, H. Wu, D. Yang, J. He, G. V. Biesold-McGee, S. Liang, W. Yen, X. Tang, J. Yeh, Z. Lin and J. He, Adv. Mater., 2020, **32**, 1906457.
26 S. C. Sevov, in Intermetallic Compounds - Principles and Practice, eds. J. H. Westbrook and R. L. Fleischer, Wiley, 2002, pp. 113–132.
27 H. Schäfer, B. Eisenmann and W. Müller, Angew. Chemie Int. Ed. Engl., 1973, **12**, 694–712.
28 T. F. Fässler, Ed., Zintl Phases, Springer Berlin Heidelberg, Berlin, Heidelberg, 2011, vol. 139.
29 A. Ovchinnikov and S. Bobev, J. Solid State Chem., 2019, **270**, 346–359.
30 S. Baranets, A. Ovchinnikov and S. Bobev, In Handbook on the Physics and Chemistry of Rare Earths, 2021, pp. 227–324.
31 R. J. Wilson, B. Weinert and S. Dehnen, Dalton Trans., 2018, **47**, 14861–14869.
32 S. Scharfe, F. Kraus, S. Stegmaier, A. Schier and T. F. Fässler, Angew. Chemie Int. Ed., 2011, **50**, 3630–3670.
33 C. Liu and Z.-M. Sun, Coord. Chem. Rev., 2019, **382**, 32–56.
34 S. M. Kauzlarich, Materials (Basel)., 2019, **12**, 2554.
35 A. V. Shevelkov and K. Kovnir, 2010, pp. 97–142.
36 S. M. Kauzlarich, A. Zevalkink, E. Toberer and G. J. Snyder, in Thermoelectric Materials and Devices, The Royal Society of Chemistry, 2016, pp. 1–26.
37 J. Shuai, J. Mao, S. Song, Q. Zhang, G. Chen and Z. Ren, Mater. Today Phys., 2017, **1**, 74–95.
38 K.-F. Liu and S.-Q. Xia, J. Solid State Chem., 2019, **270**, 252–264.
39 M. O. Ogunbunmi and S. Bobev, Chem. Mater., 2022, **34**, 8808–8814.
40 M. O. Ogunbunmi, S. Baranets and S. Bobev, Inorg. Chem., 2022, **61**, 10888–10897.
41 S. Baranets and S. Bobev, Inorg. Chem., 2019, **58**, 8506–8516.
42 S. Baranets and S. Bobev, J. Am. Chem. Soc., 2021, **143**, 65–68.
43 S. Baranets, A. Balvanz, G. M. Darone and S. Bobev, Chem. Mater., 2022, **34**, 4172–4185.
44 A. Balvanz, S. Baranets, M. O. Ogunbunmi and S. Bobev, Inorg. Chem., 2021, **60**, 14426–14435.
45 H. Li, S.-Y. Gao, S.-F. Duan, Y.-F. Xu, K.-J. Zhu, S.-J. Tian, J.-C. Gao, W.-H. Fan, Z.-C. Rao, J.-R. Huang, J.-J. Li, D.-Y. Yan, Z.-T. Liu, W.-L. Liu, Y.-B. Huang, Y.-L. Li, Y. Liu, G.-B. Zhang, P. Zhang, T. Kondo, S. Shin, H.-C. Lei, Y.-G. Shi, W.-T. Zhang, H.-M. Weng, T. Qian and H. Ding, Phys. Rev. X, 2019, **9**, 041039.
46 M. O. Ogunbunmi, S. Baranets, A. B. Childs and S. Bobev, Dalton Trans., 2021, **50**, 9173–9184.
47 S. M. Kauzlarich, S. R. Brown and G. J. Snyder, Dalton Trans., 2007, 2099–2107.
48 D. H. Fabini, M. Koerner and R. Seshadri, Chem. Mater., 2019, **31**, 1561–1574.
49 S. Azam, S. A. Khan and S. Goumri-Said, Mater. Res. Bull., 2015, **70**, 847–855.
50 R. Nesper, Z. Anorg. Allg. Chemie, 2014, **640**, 2639–2648.
51 S. R. Brown, S. M. Kauzlarich, F. Gascoin and G. J. Snyder, Chem. Mater., 2006, **18**, 1873–1877.
52 S. Ohno, U. Aydemir, M. Amsler, J.-H. Pöhls, S. Chanakian, A. Zevalkink, M. A. White, S. K. Bux, C. Wolverton and G. J. Snyder, Adv. Funct. Mater., 2017, **27**, 1606361.
53 X.-J. Wang, M.-B. Tang, H.-H. Chen, X.-X. Yang, J.-T. Zhao, U. Burkhardt and Y. Grin, Appl. Phys. Lett., 2009, **94**, 092106.
54 F. Gascoin, S. Ottensmann, D. Stark, S. M. Haïle and G. J. Snyder, Adv. Funct. Mater., 2005, **15**, 1860–1864.
55 E. S. Toberer, A. Zevalkink, N. Crisosto and G. J. Snyder, Adv. Funct. Mater., 2010, **20**, 4375–4380.
56 U. Aydemir, A. Zevalkink, A. Ormeci, S. Bux and G. J. Snyder, J. Mater. Chem. A, 2016, **4**, 1867–1875.
57 U. Aydemir, A. Zevalkink, A. Ormeci, Z. M. Gibbs, S. Bux and G. J. Snyder, Chem. Mater., 2015, **27**, 1622–1630.
58 S. Ohno, K. Imasato, S. Anand, H. Tamaki, S. D. Kang, P. Gorai, H. K. Sato, E. S. Toberer, T. Kanno and G. J. Snyder, Joule, 2018, **2**, 141–154.
59 G. S. Pomrehn, A. Zevalkink, W. G. Zeier, A. van de Walle and G. J. Snyder, Angew. Chemie Int. Ed., 2014, **53**, 3422–3426.
60 J. Shuai, Y. Wang, H. S. Kim, Z. Liu, J. Sun, S. Chen, J. Sui and Z. Ren, Acta Mater., 2015, **93**, 187–193.
61 W. Zhang, C. Chen, H. Yao, W. Xue, S. Li, F. Bai, Y. Huang, X. Li, X. Lin, F. Cao, J. Sui, S. Wang, B. Yu, Y. Wang, X. Liu and Q. Zhang, Chem. Mater., 2020, **32**, 6983–6989.
62 J. Shuai, H. Geng, Y. Lan, Z. Zhu, C. Wang, Z. Liu, J. Bao, C.-W. Chu, J. Sui and Z. Ren, Proc. Natl. Acad. Sci., , DOI:10.1073/pnas.1608794113.
63 63 A. He, S. K. Bux, Y. Hu, D. Uhl, L. Li, D. Donadio and S. M. Kauzlarich, Chem. Mater., 2019, **31**, 8076–8086.
64 64 A. Balvanz, J. Qu, S. Baranets, E. Ertekin, P. Gorai and S. Bobev, Chem. Mater., 2020, **32**, 10697–10707.
65 65 K. Rajput, S. Baranets and S. Bobev, Chem. Mater., 2020, **32**, 9616–9626.
66 S. Baranets and S. Bobev, Mater. Today Adv., 2020, **7**, 100094.
67 A. Ovchinnikov, S. Chanakian, A. Zevalkink and S. Bobev, Chem. Mater., 2021, **33**, 3172–3186.
68 M. O. Ogunbunmi, S. Baranets and S. Bobev, Mater. Today Adv., 2022, **16**, 100310.
69 M. O. Ogunbunmi and S. Bobev, Mater. Today Phys., 2022, **26**, 100725.
70 M. O. Ogunbunmi, S. Baranets and S. Bobev, Dalton Trans., , DOI:10.1039/D2DT00412G.
71 A. B. Childs, S. Baranets and S. Bobev, J. Solid State Chem., 2019, **278**, 120889.
72 B. Saparov, S. Bobev, A. Ozbay and E. R. Nowak, J. Solid State Chem., 2008, **181**, 2690–2696.
73 D. K. Wilson, B. Saparov and S. Bobev, Z. Anorg. Allg. Chemie, 2011, **637**, 2018–2025.

74 S. Bobev, V. Fritsch, J. D. Thompson, J. L. Sarrao, B. Eck, R. Dronskowski and S. M. Kauzlarich, J. Solid State Chem., 2005, **178**, 1071–1079.
75 S.-Q. Xia and S. Bobev, Inorg. Chem., 2008, **47**, 1919–1921.
76 H. He, C. Tyson, M. Saito and S. Bobev, J. Solid State Chem., 2012, **188**, 59–65.
77 A. B. Maghirang, R. A. B. Villaos, M. N. R. Perez, L.-Y. Feng, Z.-Q. Huang, C.-H. Hsu and F.-C. Chuang, ACS Appl. Electron. Mater., 2022, **4**, 5308–5316.
78 L.-L. Wang, A. Kaminski, P. C. Canfield and D. D. Johnson, J. Phys. Chem. C, 2018, **122**, 705–713.
79 T. Berry, V. J. Stewart, B. W. Y. Redemann, C. Lygouras, N. Varnava, D. Vanderbilt and T. M. McQueen, Phys. Rev. B, 2022, **106**, 054420.
80 M. N. R. Perez, R. A. B. Villaos, L.-Y. Feng, A. B. Maghirang, C.-P. Cheng, Z.-Q. Huang, C.-H. Hsu, A. Bansil and F.-C. Chuang, Appl. Phys. Rev., 2022, **9**, 011410.
81 L. Müchler, F. Casper, B. Yan, S. Chadov and C. Felser, Phys. Status Solidi - Rapid Res. Lett., 2013, **7**, 91–100.
82 N. Xu, Y. Xu and J. Zhu, npj Quantum Mater., 2017, **2**, 51.
83 R. Takahashi and S. Murakami, Semicond. Sci. Technol., 2012, **27**, 124005.
84 L. Müchler, B. Yan, F. Casper, S. Chadov and C. Felser, 2013, pp. 123–139.
85 J.-B. Vaney, S. Aminorroaya Yamini, H. Takaki, K. Kobayashi, N. Kobayashi and T. Mori, Mater. Today Phys., 2019, **9**, 100090.
86 C.-C. Zhao and C. Xiao, Rare Met., 2021, **40**, 752–766.
87 Y. Xu, Z. Song, Z. Wang, H. Weng and X. Dai, Phys. Rev. Lett., 2019, **122**, 256402.
88 D. Pesin and A. H. MacDonald, Nat. Mater., 2012, **11**, 409–416.
89 Y. Fan and K. L. Wang, SPIN, 2016, **06**, 1640001.
90 M. O. Ogunbunmi, H. S. Nair and A. M. Strydom, Crit. Rev. Solid State Mater. Sci., 2022, 1–22.
91 B. C. Sales, D. Mandrus and R. K. Williams, Science (80-.)., 1996, **272**, 1325–1328.
92 T. Zhu, C. Fu, H. Xie, Y. Liu and X. Zhao, Adv. Energy Mater., 2015, **5**, 1500588.
93 H. Kleinke, Chem. Mater., 2010, **22**, 604–611.
94 M. O. Ogunbunmi and A. M. Strydom, J. Phys. Condens. Matter, 2020, **32**, 405606.
95 R. K. Kamadurai, M. O. Ogunbunmi, H. S. Nair and A. M. Strydom, J. Alloys Compd., 2021, **872**, 159481.
96 Y. Liu, Z. Hu, M. O. Ogunbunmi, E. Stavitski, K. Attenkofer, S. Bobev and C. Petrovic, Inorg. Chem., 2022, **61**, 13586–13590.
97 H. S. Nair, M. O. Ogunbunmi, S. K. Ghosh, D. T. Adroja, M. M. Koza, T. Guidi and A. M. Strydom, J. Phys. Condens. Matter, , DOI:10.1088/1361-648X/aab1e5.
98 M. O. Ogunbunmi, B. M. Sondezi, H. S. Nair and A. M. Strydom, Phys. B Condens. Matter, 2018, **536**, 128–132.
99 Y. Liu, M. Han, Y. Lee, M. O. Ogunbunmi, Q. Du, C. Nelson, Z. Hu, E. Stavitski, D. Graf, K. Attenkofer, S. Bobev, L. Ke, Y. Zhu and C. Petrovic, Adv. Funct. Mater., 2022, **32**, 2105111.
100 Y. V. Ivanov, A. T. Burkov and D. A. Pshenay-Severin, Phys. Status Solidi Basic Res., 2018, 255, 1800020.
101 J. P. Heremans, R. J. Cava and N. Samarth, Nat. Rev. Mater., 2017, **2**, 17049.
102 R.-L. Chu, W.-Y. Shan, J. Lu and S.-Q. Shen, Phys. Rev. B, 2011, **83**, 075110.
103 M. Z. Hasan and C. L. Kane, Rev. Mod. Phys., 2010, **82**, 3045–3067.
104 M. Z. Hasan and J. E. Moore, Annu. Rev. Condens. Matter Phys., 2011, **2**, 55–78.
105 D. M. Nenno, C. A. C. Garcia, J. Gooth, C. Felser and P. Narang, Nat. Rev. Phys., 2020, **2**, 682–696.
106 K. Okamoto, K. Kuroda, H. Miyahara, K. Miyamoto, T. Okuda, Z. S. Aliev, M. B. Babanly, I. R. Amiraslanov, K. Shimada, H. Namatame, M. Taniguchi, D. A. Samorokov, T. V. Menshchikova, E. V. Chulkov and A. Kimura, Phys. Rev. B, 2012, **86**, 195304.
107 B. Singh, H. Lin and A. Bansil, Adv. Mater., 2022, 2201058.
108 A. A. Taskin and Y. Ando, Phys. Rev. B, 2009, **80**, 085303.
109 T. V. Menshchikova, S. V. Eremeev and E. V. Chulkov, Appl. Surf. Sci., 2013, **267**, 1–3.
110 L. Zhang, X.-Y. Song and F. Wang, Phys. Rev. Lett., 2016, **116**, 046404.
111 L. Müchler, H. Zhang, S. Chadov, B. Yan, F. Casper, J. Kübler, S.-C. Zhang and C. Felser, Angew. Chem. Int. Ed., 2012, **51**, 7221–7225.
112 W. Tian, W. Yu, J. Shi and Y. Wang, Materials (Basel)., 2017, **10**, 814.
113 L. Fu, C. L. Kane and E. J. Mele, Phys. Rev. Lett., 2007, **98**, 106803.
114 X.-L. Q. and S.-C. Zhang, Rev. Mod. Phys., 2011, **83**, 1057.
115 N. Kumar, S. N. Guin, K. Manna, C. Shekhar and C. Felser, Chem. Rev., 2021, 121, 2780–2815.
116 J. He, J. R. Sootsman, S. N. Girard, J.-C. Zheng, J. Wen, Y. Zhu, M. G. Kanatzidis and V. P. Dravid, J. Am. Chem. Soc., 2010, **132**, 8669–8675.
117 M. Hong, Z.-G. Chen and J. Zou, Chinese Phys. B, 2018, **27**, 048403.
118 Y. P. Zhiwei Chen, XinyueZhang, Adv. Mater., 2018, **30**, 1705617.
119 G. A. Slack, CRC Handbook of Thermoelectrics, CRC Press, Boca Raton, FL, Ch 34.
120 R. Hoffmann, Angew. Chemie Int. Ed. Engl., 1987, **26**, 846–878.
121 R. Hoffmann, Rev. Mod. Phys., 1988, **60**, 601–628.
122 B. Bradlyn, L. Elcoro, J. Cano, M. G. Vergniory, Z. Wang, C. Felser, M. I. Aroyo and B. A. Bernevig, Nature, 2017, **547**, 298–305.
123 L. M. Schoop and A. Topp, in Topological Matter, ed. M. Bercioux, D., Cayssol, J., Vergniory, M., Reyes Calvo, Springer Series in Solid-State Sciences, vol 190. Springer, Cham., 2018, pp. 211–243.
124 L. Ding, C. Hu, F. Ye, E. Feng, N. Ni and H. Cao, Phys. Rev. B, 2020, **101**, 020412.
125 R. Peng, Y. Ma, H. Wang, B. Huang and Y. Dai, Phys. Rev. B, 2020, **101**, 115427.
126 R. J. Cava, H. Ji, M. K. Fuccillo, Q. D. Gibson and Y. S. Hor, J. Mater. Chem. C, 2013, **1**, 3176.
127 H. Zhang, C.-X. Liu, X.-L. Qi, X. Dai, Z. Fang and S.-C. Zhang, Nat. Phys., 2009, **5**, 438–442.
128 L. Fu and C. L. Kane, Phys. Rev. B, 2007, **76**, 045302.
129 L. Fu, C. L. Kane and E. J. Mele, Phys. Rev. Lett., 2007, **98**, 106803.
130 Y. Pei, H. Wang and G. J. Snyder, Adv. Mater., 2012, **24**, 6125–6135.
131 J. Mao, Z. Liu, J. Zhou, H. Zhu, Q. Zhang, G. Chen and Z. Ren, Adv. Phys., 2018, **67**, 69–147.
132 N. Van Toan, T. T. K. Tuoi and T. Ono, Energy Convers. Manag., 2020, **225**, 113442.
133 Y. Du, J. Chen, Q. Meng, Y. Dou, J. Xu and S. Z. Shen, Vacuum, 2020, **178**, 109384.
134 T. H. Hsieh, H. Lin, J. Liu, W. Duan, A. Bansil and L. Fu, Nat. Commun., 2012, **3**, 982.
135 J. Zhang, C.-Z. Chang, Z. Zhang, J. Wen, X. Feng, K. Li, M. Liu, K. He, L. Wang, X. Chen, Q.-K. Xue, X. Ma and Y. Wang, Nat. Commun., 2011, **2**, 574.
136 Y. L. Chen, J. G. Analytis, J.-H. Chu, Z. K. Liu, S.-K. Mo, X. L. Qi, H. J. Zhang, D. H. Lu, X. Dai, Z. Fang, S. C. Zhang, I. R. Fisher, Z. Hussain and Z.-X. Shen, Science, 2009, **325**, 178–181.

137 Y. Pei, A. D. LaLonde, H. Wang and G. J. Snyder, Energy Environ. Sci., 2012, **5**, 7963.
138 I. T. Witting, T. C. Chasapis, F. Ricci, M. Peters, N. A. Heinz, G. Hautier and G. J. Snyder, Adv. Electron. Mater., 2019, **5**, 1800904.
139 R. P. Chasmar and R. Stratton, J. Electron. Control, 1959, **7**, 52–72.
140 G. D. Mahan, in Solid State Physics Vol. 51, ed. F. S. H. Ehrenreich, Academic Press Inc, San Diego, 1998, p. 81.
141 J. Zhu, X. Zhang, M. Guo, J. Li, J. Hu, S. Cai, W. Cai, Y. Zhang and J. Sui, npj Comput. Mater., 2021, **7**, 116.
142 F.-H. Lin and C.-J. Liu, Sci. Rep., 2022, **12**, 7056.
143 H. Naithani and T. Dasgupta, ACS Appl. Energy Mater., 2020, **3**, 2200–2213.
144 J. Yan, P. Gorai, B. Ortiz, S. Miller, S. A. Barnett, T. Mason, V. Stevanović and E. S. Toberer, Energy Environ. Sci., 2015, **8**, 983–994.
145 T. Wang, C. Zhang, H. Snoussi and G. Zhang, Adv. Funct. Mater., 2020, **30**, 1906041.
146 Y. Iwasaki, I. Takeuchi, V. Stanev, A. G. Kusne, M. Ishida, A. Kirihara, K. Ihara, R. Sawada, K. Terashima, H. Someya, K. Uchida, E. Saitoh and S. Yorozu, Sci. Rep., 2019, **9**, 2751.
147 M. W. Gaultois, A. O. Oliynyk, A. Mar, T. D. Sparks, G. J. Mulholland and B. Meredig, APL Mater., 2016, **4**, 053213.
148 C. Fu, Y. Sun and C. Felser, APL Mater., 2020, **8**, 040913.
149 J. Gooth, G. Schierning, C. Felser and K. Nielsch, MRS Bull., 2018, **43**, 187–192.
150 H. J. Goldsmid, Introduction to Thermoelectricity, Springer, New York, Vol. 121., 2009.
151 Y. Xu, Z. Gan and S.-C. Zhang, Phys. Rev. Lett., 2014, **112**, 226801.
152 P. Ghaemi, R. S. K. Mong and J. E. Moore, Phys. Rev. Lett., 2010, **105**, 166603.
153 G. Bruzzone and E. Franceschi, J. Less Common Met., 1978, **57**, 201–208.
154 Y.-H. Duan, W.-C. Hu, Y. Sun and M.-J. Peng, J. Alloys Compd., 2014, **614**, 334–344.
155 H. Pawar, N. Acharya, M. Shugani, M. Aynyas and S. P. Sanyal, 2020, p. 030438.
156 D. B. Migas, L. Miglio, V. L. Shaposhnikov and V. E. Borisenko, Phys. Rev. B, 2003, **67**, 205203.
157 S. Lebègue, B. Arnaud and M. Alouani, Phys. Rev. B, 2005, **72**, 085103.
158 J. Tani and H. Kido, Comput. Mater. Sci., 2015, **97**, 36–41.
159 D. B. Migas, V. O. Bogorodz, A. B. Filonov, V. L. Shaposhnikov, V. E. Borisenko and N. G. Galkin, Jpn. J. Appl. Phys., 2015, **54**, 07JA03.
160 P. Eckerlin and E. Wolfel, Zeitschrift fur Anorg. und Allg. Chemie, 1955, **280**, 321–331.
161 G. Bruzzone and F. Merlo, J. Less Common Met., 1976, **48**, 103–109.
162 H. Ud Din, A. H. Reshak, G. Murtaza, B. Amin, R. Ali, Z. A. Alahmed, J. Chyský, J. Bila and H. Kamarudin, Indian J. Phys., 2015, **89**, 369–375.
163 Z. Yang, D. Shi, B. Wen, R. Melnik, S. Yao and T. Li, J. Solid State Chem., 2010, **183**, 136–143.
164 M. Bischoff, D. Gudat and R. Niewa, Z. Krist., 2011, **226**, 585–589.
165 Y. Li, G. Bian and D. J. Singh, AIP Adv., 2016, **6**, 125108.
166 R. Mishra, R.-D. Hoffmann, R. Pöttgen, H. Trill and B. D. Mosel, Z. Anorg. Allg. Chemie, 2002, **628**, 741.
167 Y. Duan and Y. Sun, Sci. China Physics, Mech. Astron., 2013, **56**, 1854–1860.
168 C. B. Shoemaker and D. P. Shoemaker, Acta Crystallogr., 1965, **18**, 900–905.
169 A. K. Ganguli, A. M. Guloy and J. D. Corbett, J. Solid State Chem., 2000, **152**, 474–477.
170 P. Eckerlin, E. Leicht and E. Wolfel, Z. Anorg. Allg. Chemie, 1961, **307**, 145–156.
171 P. Manfrinetti, M. L. Fornasini and A. Palenzona, Intermetallics, 2000, **8**, 223–228.
172 Y. Sun, X.-Q. Chen, C. Franchini, D. Li, S. Yunoki, Y. Li and Z. Fang, Phys. Rev. B, 2011, **84**, 165127.
173 Z. Zhu, M. Li and J. Li, Phys. Rev. B, 2016, **94**, 155121.
174 J. Heyd, G. E. Scuseria and M. Ernzerhof, J. Chem. Phys., 2003, **118**, 8207–8215.
175 D. Parker and D. J. Singh, Sci. Technol. Adv. Mater., 2013, **14**, 055003.
176 Y. Katsura and H. Takagi, J. Electron. Mater., 2013, **42**, 1365–1368.
177 Y. Zhang, X. Ke, C. Chen, J. Yang and P. R. C. Kent, Phys. Rev. B, 2009, **80**, 024304.
178 A. Y. Vigdorovich, V.N., Nashel'skii, Russ. J. Inorg. Chem., **4**, 922–925.
179 G. Bruzzone, E. Franceschi and F. Merlo, J. Less Common Met., 1981, **81**, 155–160.
180 G. Bruzzone and E. Franceschi, J. Less Common Met., 1977, **52**, 211–216.
181 M. Idbenali, C. Servant, N. Selhaoui and L. Bouirden, Calphad, 2008, **32**, 64–73.
182 V. A. Russell and P. H. Klein, Adv. Energy Convers., 1961, **1**, 147.
183 V. K. Zaitsev, M. I. Fedorov, E. A. Gurieva, I. S. Eremin, P. P. Konstantinov, A. Y. Samunin and M. V. Vedernikov, Phys. Rev. B, 2006, **74**, 045207.
184 K. Kutorasinski, B. Wiendlocha, J. Tobola and S. Kaprzyk, Phys. Rev. B, 2014, **89**, 115205.
185 X. J. Tan, W. Liu, H. J. Liu, J. Shi, X. F. Tang and C. Uher, Phys. Rev. B, 2012, **85**, 205212.
186 G. S. Nolas, D. Wang and M. Beekman, Phys. Rev. B, 2007, **76**, 235204.
187 H. Gao, T. Zhu, X. Liu, L. Chen and X. Zhao, J. Mater. Chem., 2011, **21**, 5933.
188 J. J. Pulikkotil, D. J. Singh, S. Auluck, M. Saravanan, D. K. Misra, A. Dhar and R. C. Budhani, Phys. Rev. B, 2012, **86**, 155204.
189 W. Liu, Q. Zhang, K. Yin, H. Chi, X. Zhou, X. Tang and C. Uher, J. Solid State Chem., 2013, **203**, 333–339.
190 J. Mao, H. S. Kim, J. Shuai, Z. Liu, R. He, U. Saparamadu, F. Tian, W. Liu and Z. Ren, Acta Mater., 2016, **103**, 633–642.
191 W. Liu, X. Tang, H. Li, J. Sharp, X. Zhou and C. Uher, Chem. Mater., 2011, **23**, 5256–5263.
192 J. Tani and H. Kido, Intermetallics, 2007, **15**, 1202–1207.
193 X. Liu, T. Zhu, H. Wang, L. Hu, H. Xie, G. Jiang, G. J. Snyder and X. Zhao, Adv. Energy Mater., 2013, **3**, 1238–1244.
194 W. Liu, X. Tan, K. Yin, H. Liu, X. Tang, J. Shi, Q. Zhang and C. Uher, Phys. Rev. Lett., 2012, **108**, 166601.
195 A. M. Goforth, H. Hope, C. L. Condron, S. M. Kauzlarich, N. Jensen, P. Klavins, S. MaQuilon and Z. Fisk, Chem. Mater., 2009, **21**, 4480–4489.
196 A. M. Goforth, P. Klavins, J. C. Fettinger and S. M. Kauzlarich, Inorg. Chem., 2008, **47**, 11048–11056.
197 W.-T. Guo, Z. Huang and J.-M. Zhang, Phys. Chem. Chem. Phys., 2022, **24**, 17337–17347.
198 J. Jiang and S. M. Kauzlarich, Chem. Mater., 2006, **18**, 435–441.
199 T. Sato, Z. Wang, D. Takane, S. Souma, C. Cui, Y. Li, K. Nakayama, T. Kawakami, Y. Kubota, C. Cacho, T. K. Kim, A. Arab, V. N. Strocov, Y. Yao and T. Takahashi, Phys. Rev. Res., 2020, **2**, 033342.
200 H. A. Alburaih, S. Aman, S. Mehmood, Z. Ali, S. R. Ejaz, R. Y. Khosa, N. Ahmad, M. S. Al-Buriahi, Z. A. Alrowaili and H. M. T. Farid, Appl. Phys. A, 2022, **128**, 451.
201 J. F. Rauscher, C. L. Condron, T. Beault, S. M. Kauzlarich,

N. Jensen, P. Klavins, S. MaQuilon, Z. Fisk and M. M. Olmstead, Acta Crystallogr. C, 2009, **65**, i69–i73.
202 N. Guechi, A. Bouhemadou, Y. Medkour, Y. Al-Douri, R. Khenata and S. Bin-Omran, Philos. Mag., 2020, **100**, 3023–3039.
203 N. Guechi, A. Bouhemadou, A. Guechi, M. Reffas, L. Louail, A. Bourzami, M. Chegaar and S. Bin-Omran, J. Alloys Compd., 2013, **577**, 587–599.
204 Z. Wang, G. Wang, X. Shi, D. Wang and X. Tian, J. Phys. D. Appl. Phys., 2017, **50**, 465304.
205 H. Wang, X. Zhu, Z. Chen, F. Lu, H. Li, Y. Han, L. Li, W. Gao, W. Ning and M. Tian, J. Phys. Condens. Matter, , DOI:10.1088/1361-648X/abe96d.
206 S. Baranets and S. Bobev, J. Solid State Chem., 2021, **303**, 122467.
207 A. Wang, S. Baranets, Y. Liu, X. Tong, E. Stavitski, J. Zhang, Y. Chai, W.-G. Yin, S. Bobev and C. Petrovic, Phys. Rev. Res., 2020, **2**, 033462.
208 X. Zhang, Q. Liu, Q. Xu, X. Dai and A. Zunger, J. Am. Chem. Soc., 2018, **140**, 13687–13694.
209 Y. Pan, F. Fan, X. Hong, B. He, C. Le, W. Schnelle, Y. He, K. Imasato, H. Borrmann, C. Hess, B. Büchner, Y. Sun, C. Fu, G. J. Snyder and C. Felser, Adv. Mater., 2021, **33**, 2003168.
210 F. Yang, T. Ikeda, G. J. Snyder and C. Dames, J. Appl. Phys., 2010, **108**, 034310.
211 H.-W. Jeon, H.-P. Ha, D.-B. Hyun and J.-D. Shim, J. Phys. Chem. Solids, 1991, **52**, 579–585.
212 L. Zhang, Z. Sun, A. Wang, Y. Xia, X. Mi, L. Zhang, M. He, Y. Chai, T. Wu, R. Wang, X. Zhou and X. Chen, Phys. Rev. B, 2021, **104**, 205108.
213 R. A. Susilo, W. Deng, J. Feng, A. Wang, N. Kawamura, N. Ishimatsu, S. Kawaguchi, M. Yuan, H. Li, W. Ren, T. Nakagawa, C. Petrovic and B. Chen, Phys. Rev. Res., 2021, **3**, 043028.
214 L.-Y. Feng, R. A. B. Villaos, A. B. Maghirang, Z.-Q. Huang, C.-H. Hsu, H. Lin and F.-C. Chuang, Sci. Rep., 2022, **12**, 4582.
215 A. F. May, M. A. McGuire, D. J. Singh, J. Ma, O. Delaire, A. Huq, W. Cai and H. Wang, Phys. Rev. B, 2012, **85**, 035202.
216 S. Xu, H. Wang, Y.-Y. Wang, Y. Su, X.-Y. Wang and T.-L. Xia, J. Cryst. Growth, 2020, **531**, 125304.
217 S. K. Kang and G. J. Miller, Acta Crystallogr. Sect. E Struct. Reports Online, 2002, **58**, i21–i22.
218 M. K. Hooda, O. Pavlosiuk, Z. Hossain and D. Kaczorowski, Phys. Rev. B, 2022, **106**, 045107.
219 C. K. Barman, C. Mondal, B. Pathak and A. Alam, Phys. Rev. Mater., 2020, **4**, 084201.
220 X.-H. Qiang and L. Huang, Mod. Phys. Lett. B, 2021, **35**, 2150180.
221 C. P. Zhixiang Hu, J. Deng, H. Li, M. Ogunbunmi, X. Tong, Q. Wang, D. Graf, W. R. Pudelko, Y. Liu, H. Lei, S. Bobev, M. Radovic, Z. Wang, C. Petrovic, npj Quantum Mater, 2023, in press.
222 Z. Z. Zhou, K. L. Peng, H. X. Fu, H. Wu, G. Y. Wang and X. Y. Zhou, Phys. Rev. Appl., 2021, **16**, 064034.
223 B. Salmankurt, Phys. status solidi, 2022, **259**, 2200132.
224 F. Merlo, M. Pani and M. L. Fornasini, J. Less Common Met., 1990, **166**, 319–327.
225 W. Bockelmann and H.-U. Schuster, Z. Anorg. Allg. Chemie, 1974, **410**, 233–240.
226 J. Chen, W. Xue, C. Chen, H. Li, C. Cai, Q. Zhang and Y. Wang, Adv. Sci., 2021, **8**, 2100109.
227 J. Wang, X.-C. Liu, S.-Q. Xia and X.-T. Tao, J. Am. Chem. Soc., 2013, **135**, 11840–11848.
228 T.-C. Ma, J.-N. Hu, Y. Chen, L. Shao, X.-R. Hu and J.-B. Deng, Mod. Phys. Lett. B, 2021, **35**, 2150181.
229 Y. Huang, C. Chen, W. Zhang, X. Li, W. Xue, X. Wang, Y. Liu, H. Yao, Z. Zhang, Y. Chen, F. Cao, X. Liu, Y. Wang and Q. Zhang, Sci. China Mater., 2021, **64**, 2541–2550.
230 S.-F. Wang, Z.-G. Zhang, B.-T. Wang, J.-R. Zhang and F.-W. Wang, Chinese Phys. Lett., 2021, **38**, 046301.
231 Z. Zhou, K. Peng, S. Xiao, Y. Wei, Q. Dai, X. Lu, G. Wang and X. Zhou, J. Phys. Chem. Lett., 2022, **13**, 2291–2298.
232 K. Peng, Z. Zhou, H. Wang, H. Wu, J. Ying, G. Han, X. Lu, G. Wang, X. Zhou and X. Chen, Adv. Funct. Mater., 2021, **31**, 2100583.
233 S. Zheng, K. Peng, S. Xiao, Z. Zhou, X. Lu, G. Han, B. Zhang, G. Wang and X. Zhou, J. Adv. Ceram., 2022, **11**, 1604–1612.
234 J. Guo, M. Zhu, X. Li, X.-T. Tao and S.-Q. Xia, Inorg. Chem. Front., 2018, **5**, 1902–1911.
235 Z. K. Liu, B. Zhou, Y. Zhang, Z. J. Wang, H. M. Weng, D. Prabhakaran, S.-K. Mo, Z. X. Shen, Z. Fang, X. Dai, Z. Hussain and Y. L. Chen, Science, 2014, **343**, 864–867.
236 A. Narayan, D. Di Sante, S. Picozzi and S. Sanvito, Phys. Rev. Lett., 2014, **113**, 256403.
237 J. Xiong, S. K. Kushwaha, T. Liang, J. W. Krizan, M. Hirschberger, W. Wang, R. J. Cava and N. P. Ong, Science, 2015, **350**, 413–416.
238 Y. Sun, Q.-Z. Wang, S.-C. Wu, C. Felser, C.-X. Liu and B. Yan, Phys. Rev. B, 2016, **93**, 205303.
239 Sanjeev, M. Singh, R. Kumar, S. Srivastava and T. Kumar, J. Phys. Chem. Solids, 2022, **161**, 110416.
240 A. Parveen, E. Narsimha Rao, B. Adivaiah, P. Anees and G. Vaitheeswaran, Phys. Chem. Chem. Phys., 2018, **20**, 5084–5102.
241 Y. Wang and S. Bobev, Materials (Basel)., 2023, **16**, 202301.
242 O. Jepsen, O. and O. K. Aderson, The STUTTGART TB-LMTO-ASA program; https://www2.fkf.mpg.de/andersen/LMTODOC/LMTODOC.html.
243 J. Heyd, G. E. Scuseria and M. Ernzerhof, J. Chem. Phys., 2006, **124**, 219906.
244 E. Haque, Sustain. Energy Fuels, 2021, **5**, 2441–2450.
245 S. Zhi, J. Jia, Q. Zhang, F. Cao, X. Liu and J. Mao, Mater. Today Phys., 2022, **22**, 100618.